

Metals and Electrolytes in ECM

ECM is unlike other, well established anodic dissolution processes in that the current density is high, and the electrolyte is in motion at a high velocity, and is highly concentrated. These features of the process mean that most electrochemical data, which are concerned with low current densities, and with electrolytes which are unstirred or slowly moving, and of low concentration, cannot necessarily be related to

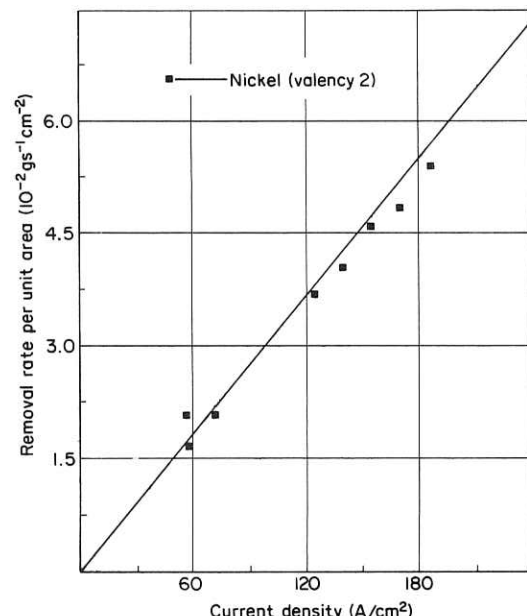


Fig. 4.1 Removal rate as a function of average current density for nickel

it. As a result, since the advent of ECM, much attention has been paid to the rates and modes of reactions at both electrodes for conditions comparable to those met in ECM; for not only must the rate at which metal is removed from the anode be sufficiently high, but also the manner of dissolution must leave an acceptable surface finish. Moreover, the progress at the anode should not receive deleterious interference from the complementary reactions at the cathode.

Although the rate of removal in theory is governed only by the local current density, in practice this rate is strongly influenced by other factors, which include the process variables and the relationship between the metal and the electrolyte. The mode of removal is similarly affected. In particular, the metal/electrolyte relationship is closely linked with the formation of surface films which play a dominant part in determining both the rate and the manner of dissolution, and with the properties of those films lies the key to good dimensional control as well as to the quality of surface finish in ECM.

4.1 Theoretical removal rates for elements

The procedure for calculating removal rates for elements has been stated in Chapter 1. If the atomic weight A and valency z of the dissolving ions are known, then Faraday's law gives the mass of metal removed, m :

$$m = \frac{AI}{zF} \quad (4.1)$$

where I is the current, t is the time of machining, and F is Faraday's constant. Thus, the rate of metal removal, \dot{m} , is

$$\dot{m} = \frac{AI}{zF} \quad (4.2)$$

It is often more convenient to work in terms of volumetric removal rates. If ρ_a is the density of the metal, from Equation (4.2) the volumetric removal rate, \dot{v} , is

$$\dot{v} = \frac{AI}{z\rho_a F} \quad (4.3)$$

Theoretical mass and volumetric removal rates for a range of elements are given in Table 4.1.

In Fig. 4.1, experimental removal rates for nickel are compared with theoretical values (based on divalent dissolution). For the

Table 4.1 Theoretical removal rates for a current of 1000 A

Metal	Atomic weight	Valency	Density (g/cm ³)	Removal rate (g/s)	$10^{-6} \text{ m}^3/\text{s}$
Aluminium	26.97	3	2.67	0.093	0.035
Beryllium	9.0	2	1.85	0.047	0.025
Chromium	51.99	2	7.19	0.269	0.038
		3		0.180	0.025
		6		0.090	0.013
Cobalt	58.93	2	8.85	0.306	0.035
		3		0.204	0.023
Niobium (Columbium)	92.91	3	9.57	0.321	0.034
		4		0.241	0.025
		5		0.193	0.020
Copper	63.57	1	8.96	0.660	0.074
		2		0.329	0.037
Iron	55.85	2	7.86	0.289	0.037
		3		0.193	0.025
Magnesium	24.31	2	1.74	0.126	0.072
Manganese	54.94	2	7.43	0.285	0.038
		4		0.142	0.019
		6		0.095	0.013
		7		0.081	0.011
Molybdenum	95.94	3	10.22	0.331	0.032
		4		0.248	0.024
		6		0.166	0.016
Nickel	58.71	2	8.90	0.304	0.034
		3		0.203	0.023
Silicon	28.09	4	2.33	0.073	0.031
Tin	118.69	2	7.30	0.615	0.084
		4		0.307	0.042
Titanium	47.9	3	4.51	0.165	0.037
		4		0.124	0.028
Tungsten	183.85	6	19.3	0.317	0.016
		8		0.238	0.012
Uranium	238.03	4	19.1	0.618	0.032
		6		0.412	0.022
Zinc	65.37	2	7.13	0.339	0.048

current densities shown (from about 60 to 186 A/cm²) removal rate was independent of flow-rates in the range 0.38×10^{-3} to 1.47×10^{-3} m³/s. Note that, as the current density is increased, the experimental rates become less than the theoretical rates. Explanations for this effect are discussed below in the section on current efficiency.

In the calculation of theoretical removal rates, confusion often arises if an incorrect valency state is attributed to the dissolving ion. For instance, nickel usually dissolves in the divalent state in nitrate and chloride solutions at low potential differences, but at higher potential differences it has been known to dissolve in the trivalent state [1].

The behaviour of copper serves as another example. This metal has been observed to dissolve in monovalent form in chloride solutions, and in the divalent state in nitrate solution [2].

Even this observation, however, needs qualification since the apparent valency of dissolution of copper changes with the mode of dissolution [3]. In nitrate and sulphate solutions copper dissolves in the active mode with an apparent valency of 2. For conditions of transpassive dissolution, the apparent valency has been found to lie between 1 and 2, e.g. 1.6 at 60 A/cm², the solution velocity being 6.86 m/s. This drop in apparent valency has been attributed to the simultaneous formation of monovalent copper reaction products. In chloride electrolytes, monovalent dissolution takes place in the active mode. For passivation conditions, the apparent valency increases, e.g. to a maximum value of 1.4 at 20 A/cm² and 6.06 m/s before reaching a limiting value of 1.2 at 40 A/cm² and 6.06 m/s. This increase is consistent with the copper dissolving partly in the divalent state. (Evidence of divalent dissolution was deduced from examination of the dissolution products. These appeared to be Cu₂O.)

4.2 Theoretical removal rates for alloys

Calculation of the removal rate for an alloy is more difficult than that for an element because the electrochemical equivalent of the alloy is not readily known. Although the electrochemical equivalents of the individual constituents of the alloy may be available, a difficulty arises in choosing a value for the electrochemical equivalent which is representative of the whole alloy. The problem has been

considered by several workers [2, 4, 5]. The two methods which have been most commonly used are the 'percentage by weight' method and the 'superposition of charge' method.

Suppose first that an alloy consists of $X_A\%$ of element A, whose atomic weight is A_A and whose ions are known to dissolve in valency state z_A , of $X_B\%$ of element B with atomic weight and valency A_B and z_B respectively, and of $X_C\%$ of element C, etc.

4.2.1 'Percentage by weight' method

The sum of the chemical equivalents (A_i/z_i) of each element, i, in the alloy, multiplied by its respective proportion by weight X_i , gives a value for the chemical equivalent of the alloy, $(A/z)_{\text{alloy}}$. Thus

$$\left(\frac{A}{z}\right)_{\text{alloy}} = \frac{1}{100} \left[X_A \left(\frac{A_A}{z_A} \right) + X_B \left(\frac{A_B}{z_B} \right) + X_C \left(\frac{A_C}{z_C} \right) + \dots \right] \quad (4.4)$$

The mass removal rate can then be found from Faraday's law:

$$\dot{m} = \left(\frac{A}{z}\right)_{\text{alloy}} \frac{I}{F}$$

4.2.2 'Superposition of charge' method

With this method, Faraday's law is used to calculate the amount of electrical charge required to dissolve the mass contribution of each constituent element to a defined mass (taken as 1 g) of the alloy.

Thus, for element A, the electrical charge required to dissolve the mass contribution ($X_A/100$) g to 1 g of the alloy is

$$\frac{X_A}{100} \left(\frac{z_A}{A_A} \right) F \text{ coulomb}$$

Similarly, for element B, the equivalent electrical charge is

$$\frac{X_B}{100} \left(\frac{z_B}{A_B} \right) F \text{ coulomb} \quad (4.5)$$

and so on, for elements C, D, etc.

The electrical charge required to dissolve 1 g of the alloy is

$$\left(\frac{z}{A}\right)_{\text{alloy}} F \text{ coulomb} \quad (4.6)$$

Equating the sum of the charge for the elements [Equation (4.5)] to the charge for the alloy [Equation (4.6)], we obtain

$$\left(\frac{z}{A}\right)_{\text{alloy}} F = \frac{F}{100} \left[X_A \left(\frac{z_A}{A_A} \right) + X_B \left(\frac{z_B}{A_B} \right) + \dots \right]$$

That is,

$$\left(\frac{A}{z}\right)_{\text{alloy}} = 100 \left[\frac{X_A}{(A_A/z_A)} + \frac{X_B}{(A_B/z_B)} + \dots \right] \quad (4.7)$$

Example

Nimonic 75 has the constituent elements with the percentage by weight given in Table 4.2. The chemical equivalent for the alloy can

Table 4.2 Constituent elements (with their percentages by weight and chemical equivalents) of Nimonic 75

Element	Ni	Cr	Fe	Ti	Si	Mn	Cu
Percentage by weight (X)	72.5	19.5	5.0	0.4	1.0	1.0	0.5
Atomic weight (A)	58.71	51.99	55.85	47.9	28.09	54.94	63.57
Valency (z)	2	3	2	2	4	2	1
Chemical equivalent (A/z)	29.36	17.34	27.93	23.95	7.02	27.47	63.57
Product $X(A/z) \times 10^{-2}$	21.286	3.381	1.396	0.096	0.070	0.275	0.318
Quotient $X/(A/z)$	2.47	1.12	0.18	0.02	0.14	0.04	0.01

(Note: Nimonic 75 also contains 0.1% of carbon, which is inert)

now be calculated. By the first method, on the addition of the quantities

$$\sum_i X_i \left(\frac{A_i}{z_i} \right)$$

the chemical equivalent is calculated to be 26.8. By the second method, the addition of the quotients

$$100 / \sum_i \frac{X_i}{(A_i/z_i)}$$

yields a value of 25.1. Little difference is apparent in the values for each calculation. But for another alloy, Monel, whose constituents

Table 4.3 Constituent elements of Monel

Element	Ni	Cu	Fe	Mn	Si	C
Percentage by weight (X)	63	31.7	2.5	2	0.5	0.3
Chemical equivalent (A/z)	29.36	63.57	27.93	27.47	7.02	—
Product $X(A/z) \times 10^{-2}$	18.5	20.2	0.70	0.55	0.04	—
Quotient $X/(A/z)$	2.15	0.50	0.09	0.07	0.07	—

are given in Table 4.3, the calculations produce 39.9 and 34.7 respectively for its chemical equivalent. This discrepancy is indicative of the caution that is required in calculations by these methods. Moreover, their use in the prediction of machining rates for alloys requires a number of assumptions which again include knowledge of the valency states on dissolution of the constituent elements. The methods do not account for the effects of process variables, for

Table 4.4 Experimental and theoretical removal rates for Nimonic 75 alloy

Current density (A/cm ²)	Machining rates (g min ⁻¹ cm ⁻²)		
	observed	theoretical	
		percentage by weight method	superposition of charge method
9.3	0.15	0.155	0.145
11.6	0.18	0.193	0.181
14	0.22	0.233	0.219
23.2	0.36	0.387	0.363

example, current density and flow-rate, on the rate of metal removal. As an example, however, some experimental results for Nimonic 75 are quoted in Table 4.4. The applied voltage was 12 V, and a 20% (w/w) NaCl solution, flowing at rates between 0.38×10^{-3} and 1.47×10^{-3} m³/s, was used; no variation in removal rate due to rate of flow was observed over this range. Although there is a slight divergence, the table shows reasonable agreement between predicted and experimental removal rates.

4.3 Current efficiency

In the previous section, a difference in theoretical and experimental removal rates was noted. This result is often met in ECM. When the cause stems from the use of current for purposes other than metal removal, then a quantitative description can be obtained from *current efficiency* values. The current efficiency is defined as the ratio of the observed amount of metal dissolved to the theoretical amount predicted from Faraday's law, for the same specified conditions of electrochemical equivalent, current, etc.

If the metal ions dissolve in one valency form z , at current I , we can write

$$\text{Current efficiency} = \frac{\dot{m}}{(A/zF)I}$$

where \dot{m} is now the observed mass removal rate corresponding to the specified experimental conditions.

It is often convenient to express the current efficiency in terms of a percentage ratio. For an efficiency of 100%, the entire current is used to dissolve the metal in accordance with Faraday's law. For zero efficiency, the current passes without metal dissolution.

Apparent current efficiency values, of course, can be affected by other factors. Since the valency states of ions can vary from solution to solution, or on alteration of a process variable, then clearly, the choice of the wrong valency can lead to an inaccurate estimate of the current efficiency. (From the example in Section 4.1, in which copper has been observed to dissolve in mono- and di-valent form, the estimated efficiency could be in error by 100%.) When alloys are machined, estimated values for their electrochemical equivalents must be used to estimate the current efficiency. We have seen that, with the usual methods of calculations, the valency values assumed

for the individual constituents of the alloys can be a possible source of error.

Passivation can also reduce the current efficiency by reducing the metal removal rate. In other cases, grain boundary attack may occur causing removal of grains of metal from the anode surface by the traction forces of the electrolyte flow. Then, the metal removal rate and the corresponding current efficiency can be increased.

Gas evolution at the anode is another common reason for erroneous estimates of efficiency. In some cases, the generation of gas at the anode can be associated with an increase in current density. Thus, at low current densities, if little or no gas is evolved at the anode, the current efficiency should be high. But, at higher current densities, more gas will be evolved, more current will be used in its generation, and the current efficiency will be accordingly reduced. In other cases, however, an increase in current density leads to an increase in current efficiency. Moreover, for a specified set of process conditions, but with a change of electrolyte, widely different current efficiency values for one metal can be obtained. Examples to illustrate these points are set out below.

4.3.1 Effects of current density and solution flow on current efficiency

The results shown for nickel in Fig. 4.1 can now be presented in terms of current efficiency values (Fig. 4.2). Note that the current efficiency decreases slightly with an increase in current density. This trend has been reported for other metals in NaCl solutions.

Cuthbertson and Turner [6], who have machined Nimonic 80 in saturated NaCl, estimate, by the percentage by weight method, that the current efficiency decreases from 82% at 15.5 A/cm^2 to

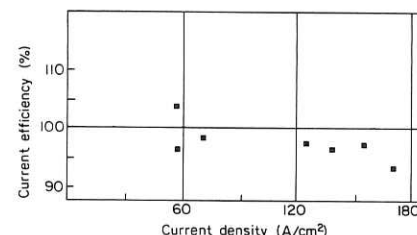


Fig. 4.2 Current efficiency as a function of current density for nickel

76% at $46.5\text{ A}/\text{cm}^2$, the electrolyte velocity being 2.85 m/s . They also report a slight increase in current efficiency with electrolyte velocity from 74% at 1.26 m/s to 76% at 2.85 m/s (for a current density of $46.5\text{ A}/\text{cm}^2$). The current efficiency for copper in 20%

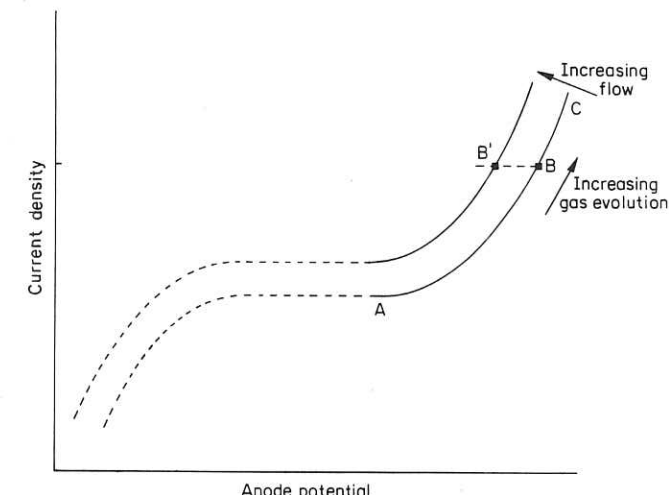


Fig. 4.3 Idealised polarisation curve

(w/w) NaCl also has been noted to increase with flow-rate up to a limiting value, e.g. at $6.96\text{ A}/\text{cm}^2$, 92% for a flow-rate of $0.96 \times 10^{-3}\text{ m}^3/\text{s}$, above which rate no further effect of flow-rate on efficiency was obtained [2]. During this investigation, no ECM was possible below a lower limiting flow-rate, owing to electric 'shorting' across the gap. (Severe mass transfer limitations on copper dissolution have been the subject of other more detailed studies [3].) A decrease in current efficiency with an increase in current density for mild steel in 2M and 4M NaCl has also been found by Mao [7], from about 99% at $26\text{ A}/\text{cm}^2$ to 94% at $62\text{ A}/\text{cm}^2$. He also reports that the cathodic efficiency for hydrogen generation is 100%.

These types of behaviour can be interpreted in terms of the polarisation curves which were introduced in Chapter 3. For convenience, an idealised curve is again given here (Fig. 4.3). In the region of A, only metal dissolution is supposed to occur. As the current density is increased along ABC, the anode potential also increases, and the higher energy then made available allows other, higher-energy electrode reactions, e.g. oxygen evolution, to occur.

Since the gas evolves in preference to metal dissolution, and in progressively greater quantities along ABC, the current efficiency for metal removal decreases. For a given current density, say at B, the effect of an increase in flow-rate, however, is the translation of the point B to B'. The latter point corresponds to a lower anode potential, so conditions are again less conducive to gas evolution. Accordingly, the current efficiency for metal removal is increased. This behaviour is not necessarily characteristic of all metal-electrolyte combinations. For instance, for a nickel-chromium alloy machined in NaClO_3 , NaNO_3 , NaNO_2 , Na_2SO_4 , and $\text{Na}_2\text{Cr}_2\text{O}_7$ electrolytes, an increase in current efficiency with current density has been reported [8].

Similar observations have been made by Bergsma [9] for steel in NaClO_3 , and by Mao for mild steel in NaClO_3 , NaClO_4 , and NaNO_3 solutions [7, 10]. The latter's experiments are discussed below.

4.3.2 Effects of different electrolytes on current efficiency

(a) Mild steel and NaClO_3 solution

Current efficiency studies for both the dissolution of metal and the generation of gas in NaClO_3 electrolyte are summarised in Tables 4.5

Table 4.5 Current efficiency values for mild steel machined in NaClO_3 ; air atmosphere; electrolyte flow-rate $0.03 \times 10^{-3} \text{ m}^3/\text{s}$ (after Mao [10])

NaClO_3 concentration (M)	Cathode material	Apparent current density (A/cm^2)	Current efficiency for H_2 generation		Divalent iron dissolution (assumed)	
			Current efficiency (%)	Current efficiency (%)	Current from	Current to
4.5	Brass	47	98.2	74.8	7.7	7.4
4.5	Pt	47	98.1	80.7	—	—
4.5	Brass	47	96.7	82.9	—	—
4.5	Pt	47	99.3	78.6	8.1	6.1
4.5	Brass	26	99.0	58.6	7.9	6.5
4.5	Pt	26	99.0	60.7	7.3	6.3
4.5	Brass	26	99.8	62.7	8.5	6.3
4.5	Pt	26	98.6	68.8	8.1	5.7
2.0	Brass	47	98.7	60.4	7.9	6.4
2.0	Brass	47	99.9	67.1	7.5	5.2
2.0	Brass	37	98.3	46.3	7.0	6.0
2.0	Brass	37	100.9	59.7	7.4	6.8

and 4.6. These experiments were carried out in cell atmospheres of both air (Table 4.5) and nitrogen (Table 4.6). A nitrogen atmosphere was also used so that the quantity of anodic oxygen would be detected, as well as metal removal.

Table 4.6 Current efficiency values for mild steel machined in NaClO_3 ; nitrogen atmosphere; brass cathode; electrolyte flow-rate $0.03 \times 10^{-3} \text{ m}^3/\text{s}$ (after Mao [10])

NaClO_3 concentration (M)	Apparent current density (A/cm^2)	Current efficiency for H_2 generation		Current efficiency for O_2 generation		Total current efficiency for O_2 and Fe (%)	Divalent iron dissolution (assumed)	
		(%)	(%)	(%)	(%)		pH change from to	
4.5	47	98.6	24.8	78.6	103.4	8.4	5.7	
4.5	37	97.2	27.4	72.6	100.0	8.2	6.7	
4.5	26	98.8	35.3	64.3	99.6	7.8	6.8	
4.5	12	100.1	57.9	41.7	99.6	8.2	7.2	
2.0	47	98.7	37.5	63.4	100.9	6.2	5.8	
2.0	37	98.1	39.5	61.0	100.5	6.4	6.2	
2.0	12	101.2	80.8	19.1	99.9	6.5	6.2	

Several significant conclusions can be made from these experiments. First, the results show that the cathodic reaction is essentially hydrogen evolution and that the current efficiency is not influenced by the two cathode materials. Next, from Table 4.6, the formation of oxygen takes place at the anode in addition to metal dissolution (probably ferrous iron). Also, during these experiments, NaCl was formed or NaClO_3 reduced, the probable overall chemical reaction being $6\text{Fe}^{++} + \text{NaClO}_3 + 3\text{H}_2\text{O} \rightarrow 6\text{Fe}^{+++} + \text{NaCl} + 6\text{OH}^-$.

Mao claims that these results are largely determined by an iron oxide film on the anode surface [10]. The film is assumed to be porous to allow the rapid passage of cations through it, with the pores small and randomly distributed. Nevertheless, the film also acts as a barrier which hinders the movement of the reaction product (the ferrous ion). The rate of metal removal is thereby decreased, the extent of decrease being dependent on the film thickness. With diminished metal removal, part of the current is used for the generation of oxygen, the possible electrode reaction being



The properties of the anode film can be explored further with the aid of Table 4.6 and Fig. 4.4. Their data show that the current efficiency for metal removal increases with current density, with a corresponding decrease in current efficiency for oxygen generation.

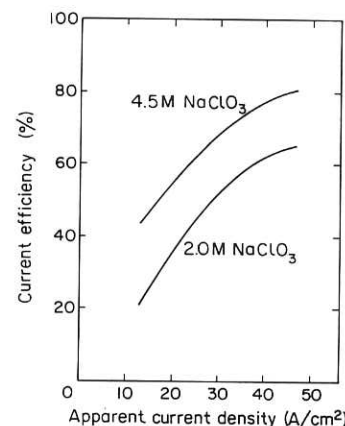


Fig. 4.4 Current efficiency for divalent iron dissolution as a function of current density (after Mao [10])

Mao suggests that as the current density is increased the thickness of the oxide film becomes thinner, so that the metal removal rate is increased. Since iron oxide is known to be more soluble at low pH, the decrease in film thickness could be caused by a locally lower pH value in the vicinity of the anode surface. That condition could be produced by the formation there of oxygen and ferrous, or ferric, hydroxide.

One other result is of interest from that study. Figure 4.5 shows that the addition of NaClO₄ to the main NaClO₃ electrolyte increases the current efficiency. The oxide film clearly must have been influenced by the effective concentration of the new electrolyte solution. The main effect of the additive is to lower the oxidising power (or the useful concentration) of the NaClO₃ solution. At high concentrations of the additive, however (above 0.25M), another feature of NaClO₄ becomes evident. At these concentrations, the NaClO₄ itself attacks the oxide film, causing pitting. At concentrations of about 0.5M, severe grain boundary attack leads to current efficiencies in excess of 100%. These results will be discussed further in relation to surface finish.

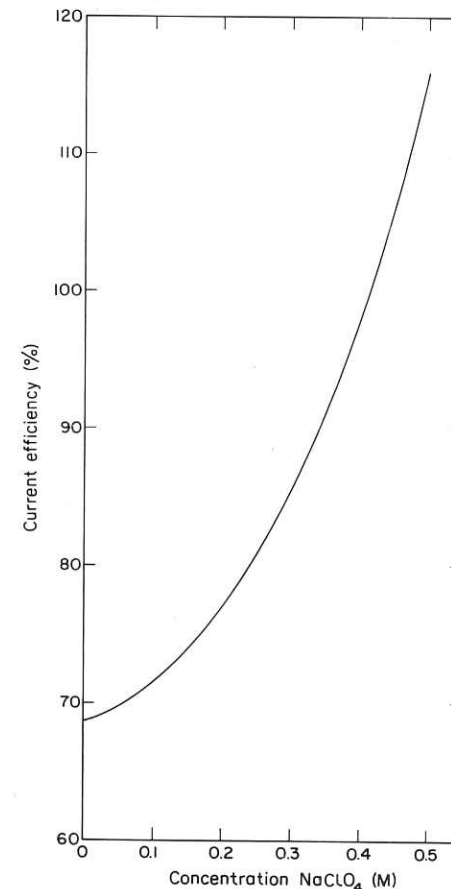


Fig. 4.5 Effect on current efficiency of ClO₄ ions added to 3M NaClO₃ electrolyte; current density 37 A/cm² (after Mao [10])

(b) Mild steel and NaClO₄ and NaNO₃ solutions

The above studies have led Mao to investigate the ECM of mild steel in other electrolytes with different oxidising strengths [7]. For example, he has found that, in 2.0M and 4.5M NaClO₄ solution and for current densities ranging from 26 to 47 A/cm², the cathode current efficiency for hydrogen generation is approximately 100%. At the anode, the current efficiencies for metal removal and oxygen generation are about 90% and 4 to 8% respectively, the total anode current efficiency being about 96%. The smaller amount of oxygen generated in NaClO₄ compared with NaClO₃ is probably due to a weaker oxide film in the former solution and to its removal by the

powerful perchlorate ions. Nevertheless, since a little oxygen is still formed during ECM, some residual oxide film must still be present. Total anode current efficiencies lower than 100% suggest that some oxygen is also used to oxidise the ferrous product of reaction. (Additional evidence has suggested that the final product is Fe_3O_4 .)

Table 4.7 Current efficiency values for mild steel machined in NaNO_3 and nitrogen atmosphere (after Mao [7])

		Divalent iron removal (assumed)							
NaNO_3 concentration (M)	Cathode	Apparent current density (A/cm ²)	Current efficiency for H ₂ generation (%)	Current efficiency for O ₂ generation (%)	Current efficiency (%)	Total current efficiency for O ₂ and Fe (%)	pH change		
							from	to	
4.5	Pt	47	1.1	54.7	33.2	87.9	5.3	11.4	
4.5	Brass	47	0	55.9	33.0	88.9	6.3	11.3	
4.5	Brass	26	0	50.6	36.8	87.4	6.2	11.2	
4.5	Brass	12	0	96.4	1.9	98.3	5.7	11.2	
2.0	Pt	47	11.6	83.7	11.7	95.4	6.0	11.4	
2.0	Brass	47	0	84.5	11.5	96.0	6.1	11.4	
2.0	Brass	26	0	96.9	2.7	99.6	6.1	11.5	

The performance of NaNO_3 electrolyte is quite different from that of the previous electrolytes (Table 4.7). No hydrogen is generated at a brass cathode, and only a small amount of the gas is formed when the cathode material is platinum. The alternative cathodic reaction appears to be reduction of nitrate, in which case ammonia, hydroxylamine, and nitrite are detected in the NaNO_3 solution after ECM.

The current efficiency for metal removal is much lower than that for NaClO_3 , and most of the current is used for the evolution of oxygen at the anode. From these results, the oxide film in NaNO_3 would appear to be less porous than that in NaClO_3 . These experiments also show that the current efficiency for iron removal in NaNO_3 increases with electrolyte concentration and with current density. Explanations for these effects are given above in the section on NaClO_3 . Since the total anode current efficiency for iron removal and oxygen generation is less than 100%, either some iron may be

dissolved as ferric ions, or some oxygen is used in oxidising the products of reaction to produce ferric hydroxide.

(c) *Mild steel and NaNO_3 solution containing additives*

Chikamori and Ito [11] have also reported that the current efficiency for mild steel machined in NaNO_3 solution increases with increasing current density, and that the metal removal rates are significantly less than those achieved in NaCl and NaClO_3 electrolytes. They believe that additives to the main solution which have oxygen-containing anions should give improved performance at higher current densities. Some results, presented in Table 4.8, do show a general

Table 4.8 Removal rates for mild steel; electrolyte velocity 8.3 m/s; temperature 40°C (after Chikamori and Ito [11])

Electrolyte	Metal removal rate (mg/C)			Specific conductivity ($\text{ohm}^{-1}\text{cm}^{-1}$ at 20°C)	pH
	Current density 25 A/cm ²	Current density 7.5 A/cm ²	Current density 2.5 A/cm ²		
100 g/l NaCl	0.286	0.297	0.292	0.119	4.7
300 g/l NaClO_3	0.257	0.200	0.098	0.132	6.2
200 g/l NaNO_3	0.104	0.011	0.004	0.126	7.5
300 g/l NaNO_3	0.142	0.022	0.006	0.156	8.2
Additive (g/l) to 200 g/l NaNO_3					
$(\text{NH}_4)_2\text{SO}_4$	30	0.181	0.064	0.143	5.6
	100	0.197	0.084	0.180	5.4
NaBrO_3	30	0.176	0.027	0.004	0.127
	100	0.200	0.036	0.008	0.135
KBrO_3	30	0.170	0.028	0.006	0.131
	100	0.200	0.053	0.006	0.146
Na_2SO_4	30	0.163	0.053	0.030	0.133
	100	0.179	0.073	0.036	0.142
$\text{Na}_2\text{Cr}_2\text{O}_7, 2\text{H}_2\text{O}$	30	0.162	0.027	0.008	0.132
	100	0.184	0.040	0.010	0.143
NaClO_3	30	0.160	0.042	0.008	0.133
	100	0.272	0.182	0.030	0.148
NH_4NO_3	30	0.150	0.013	0.008	0.145
	100	0.176	0.025	0.022	0.192
$(\text{NH}_4)_2\text{S}_2\text{O}_8$	1	0.140	0.037	0.041	0.126
NaCl	30	0.091	0.027	0.107	7.6
	100	0.033	0.032	0.296	0.184

increase in removal rates. However, the addition of NaCl has the effect of increasing removal rates at low current densities and decreasing the rates at higher current densities. In this case, an undesirable feature is a poorer surface finish.

4.4 Power efficiency

Although current efficiency is a commonly used quantity in ECM work, a more accurate evaluation of the process should include an estimate of its electrical power efficiency.

The estimate can be based on the calculation of the power required to pass a specified current across the machining gap. Since the current is fixed, only the voltage component of the power needs consideration. Now, in Chapter 3, the voltage drop across an ECM cell was shown to be composed of a main resistance drop (IR) across the gap, with other supplementary contributions which include the overpotentials at both electrodes. The resistance drop being inversely proportional to the electrolyte conductivity, a study of some relevant features of the latter quantity should show means of lessening power requirements in ECM.

One characteristic which is often utilised in practice is the rapid increase in electrolyte conductivity with temperature (40 to 60°C are common working temperatures). For some electrolytes, the conductivity can be increased two-fold for a relatively small change in temperature (e.g. from 20°C to 40°C). Therefore, for the same operating conditions, the voltage, and hence the power required, are decreased by equivalent amounts. In these cases, substantial increases in the power efficiency of the process are achieved.

Conductivity values, of course, also vary greatly with concentration, from one electrolyte to another, and even on the addition to one main electrolyte of a small quantity of some other solution. For instance, suppose that 25 V is required for the passage of 1 kA in 10% NaCl electrolyte (conductivity, $\kappa_e = 0.1 \text{ ohm}^{-1} \text{ cm}^{-1}$) at 18°C. In 20% NaCl electrolyte ($\kappa_e = 0.2 \text{ ohm}^{-1} \text{ cm}^{-1}$), 12.5 V are needed, whilst in a solution of 15% NaCl containing 1% Na_2CO_3 , 15 V are required. In the first case, the power required is 25 kW, in the second, 12.5 kW, and in the third case 15 kW.

It should be remembered, however, that electrolytes of extremely high conductivity tend to be very acidic or alkaline. Their use in practice is limited; for instance, with the acidic type, corrosion

problems make them difficult to handle. For this reason, neutral solutions, which have lower conductivities, are more common.

Also, the presence of the products of machining within the gap can influence the effective conductivity of any solution. Their detrimental effects can usually be lessened by an increase in the electrolyte flow-rate.

4.5 Types of surface finish

Many of the factors which influence the rate of dissolution also affect the manner in which metal is removed from the anode, and hence they partly determine the surface finish. Of these factors, the anode potential and current density play a major part. Their rôle can be usefully studied from polarisation curves. Information which these curves supply on the different grades of surface finish likely to be found in ECM, and examples where they are met in

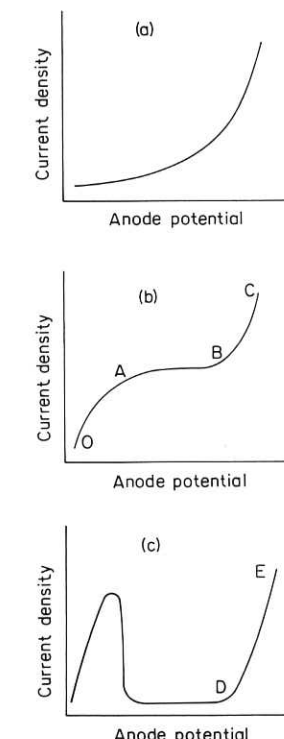


Fig. 4.6 Anode potential-current density polarisation curves

practice, are now discussed. During this discussion, it will become clear that anodic films greatly influence the quality of surface finish.

4.5.1 Etching

When etching occurs, the anode potential-current density curve usually has the form shown in Fig. 4.6(a). An explanation for etching, relevant to ECM, has been given by Boden and Brook [12]. Suppose that the individual atoms of a metal can be assumed to be spherical and simply arranged, and that the individual crystals of the metal, which are formed by the atomic lattice, can take almost any orientation of that lattice [Fig. 4.7(a)]. Slight, local variations in dissolution rates then occur, with metal dissolving more rapidly from areas which have a wider atomic spacing. Eventually, an uneven surface is produced, the exposed face having the structure of the most closely spaced atoms. On further dissolution, these close-packed layers of atoms are also removed, and the grains become disjunctive. If the grain boundaries are dissolved at a faster rate than their surrounds, as indeed often happens, entire grains can be dislodged from the metal surface. The etched finish of the metal arises from the non-specular reflection of light from the crystal faces so dissolved

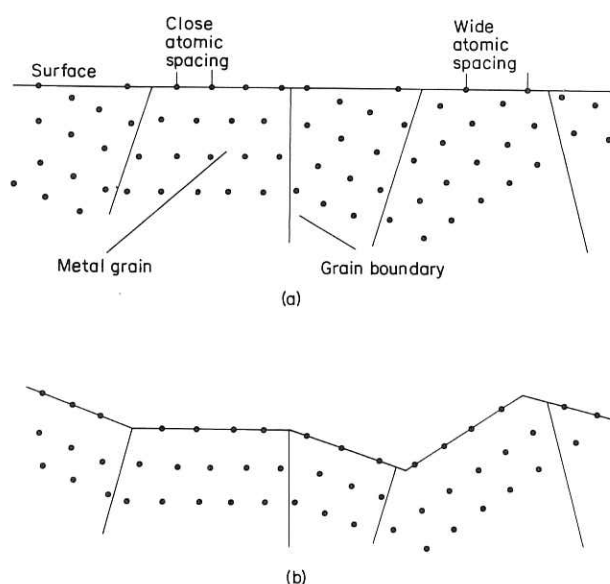


Fig. 4.7 Structure of a metal surface produced by (a) mechanical polishing, (b) mechanical polishing, then etching

at different rates. The anodic processes which lead to etching are commonly said to be 'activation-controlled'. We have already noted that Tafel's equation is usually assumed to be valid for etching conditions.

A detailed study of the active dissolution of copper in 2M KNO₃ has emphasised that crystal orientation has considerable bearing on the development of etched surface finishes [13]. Dissolution here proceeded by the removal of atoms from close-packed planes of the crystal lattice. This manner of metal removal led to a structure of surface ridges, formed by sub-microscopic steps on the metal surfaces. From this configuration, the etched appearance of the metal was obtained. This investigation also confirmed that flow-rate has no effect on this type of finish.

Etched matt finishes of approximate roughness 0.9 to 1.4 µm at current densities and electrolyte flow-rates of 15.5 A/cm² and 28 m/s respectively have been produced on Nimonic 80 machined in saturated NaCl solution [6].

4.5.2 Polishing

Figure 4.6(b) shows the usual shape of the polarisation curve for polishing conditions. Over the region OA, etching still occurs. But over the region AB, the anode surface becomes covered with a film and a polished finish results.

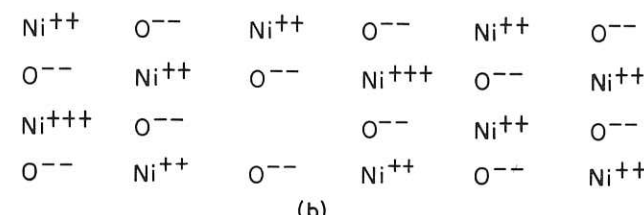
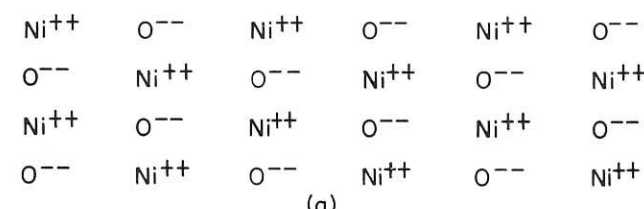


Fig. 4.8 (a) Ideal structure of NiO. (b) Real structure of NiO showing vacancy and trivalent nickel

The nature of the mechanism controlling electropolishing is still not clear, although the random removal of atoms from the surface seems the main cause. That process can be explained in terms of a 'solid defect structure' on the anode surface [12]. (A defect structure is an arrangement of ions which includes holes or vacancies in the ionic lattice by means of which ions migrate.) The structure of nickel oxide provides a convenient example. Its simple, complete structure, shown in Fig. 4.8(a) gives the formula NiO. However, from chemical analysis, its true formula can be shown to be approximately Ni_{1-r}O where $r \approx 0.05$. That is, there is a minor deficiency of metal. The discrepancy can be explained by the formation of a few Ni^{+++} (nickelic) ions and an equivalent number of vacancies, so that electrical neutrality is maintained. The structure of the oxide in this condition is given in Fig. 4.8(b).

Suppose now that, on the dissolution of a nickel anode, the metal becomes covered with such a layer of nickel oxide. Dissolution will proceed by means of the transport of ions across the oxide. We assume further that dissolution conditions (for example, the formation of a nickelic ion) also lead to the presence of a vacancy in the lattice at the oxide-solution interface. Movement of this vacancy towards the metal-oxide interface will be equivalent to the movement of metal ions in the opposite direction. On the arrival of the vacancy at the metal-oxide interface, an atom from the metal enters the vacancy and becomes charged. This arrival of the vacancy at the interface is a random process and is therefore independent of crystal orientation. The metal, accordingly, also dissolves in a random fashion, and a level surface is obtained. An electropolished surface finish will be achieved, provided that the film's properties facilitate sufficiently the movement of metal ions through the lattice. The electron conductivity of the film must also be sufficiently high to permit the process to proceed at low anode potentials.

Although these properties are not normally encountered in oxide films, some films which do contain anions other than oxygen do have the requisite properties. Boden and Brook consider that these foreign anions penetrate the film under the influence of the electrostatic field across the oxide-solution interface, thus distorting the film. They also believe that the film must be assumed to be solid, to explain the random removal of metal, and that the assumption of a lattice distorted by foreign anions in the solution is necessary for the explanation of rapid ionic transport through the film.

Beyond the solid film, a viscous layer is maintained due to the high concentration of anions and cations. The thickness of this layer, of course, depends on the rate of diffusion into the bulk of the electrolyte and on the electrolyte flow-rate (see Chapter 3). The formation of the layer is also influenced by the current density. At low current densities, the cations may diffuse away from the anode surface at a rate greater than that at which they are produced by dissolution. The concentrated layer, essential for film formation, is not produced, and etching results [Fig. 4.6(a)]. At high current densities, the process is diffusion-controlled, and a current density plateau region is obtained, as indicated in Fig. 4.6(b). The anode surface is then electropolished. Cuthbertson and Turner [6] have reported that Nimonic 80 polishes at 46.5 A/cm^2 and 28.5 m/s in saturated NaCl (surface roughness $0.2 \mu\text{m}$ CLA). They conclude that ECM must have been controlled by a viscous diffusion layer on the anode surface.

4.5.3 Polishing with pitting

At higher potentials [along BC in Fig. 4.6(b)] the polishing action is accompanied by pitting of the surface. The latter effect can be attributed to the onset of gas evolution at the anode surface, and to rupture (in some way not yet fully established) of the anodic layer by the gas. Small, fixed active sites form on the metal surface which give rise to pitting.

4.5.4 Passivation

When passivation occurs, the anodic polarisation curves take the characteristic shape, shown in Fig. 4.6(c).

Hoar [14] considers the principal action in passivation to be the very rapid formation of an oxide layer which becomes firmly attached to the metal and which forms a barrier between it and the solution. The solid film so produced has a low ionic conductivity so that the rate of dissolution of metal is decreased (partial passivation) or made negligible (total passivation). It is thought that passivating films can be either very poor electron conductors [14] or good electron conductors [15].

Total passivation with anodic gas evolution, encountered during polarisation studies of carbon steel in NaNO_3 electrolyte, has been attributed to an electronically conducting passive layer on the anode surface [16]. But an electronically non-conducting passive film is

the proposed reason for total passivation without gas generation in further work with this metal in aqueous potassium fluoride electrolyte.

The passive oxide film, which makes titanium so useful as a corrosion resistant material, renders the ECM of this metal very difficult. With simple chloride and nitrate electrolytes, high applied potential differences, e.g. 50 V, are often required to achieve machining although the passive films are then broken only at weak points causing deep attacks at grain boundaries. Even so, the power efficiency of the process is greatly reduced, and high electrolyte flow-rates are required to maintain reasonable temperatures within the gap.

It has been claimed that the voltage required to break down the passive film can be reduced by the use of bromide and iodide electrolytes, e.g. 3M NaBr and NaI [1, 17]. Even then, however, a severely pitted surface finish is obtained. An equally poor finish has been found with titanium alloy dissolved in 3M NaCl [17]. The achievement of machining in that case has been attributed to possible hydrogen gas generation at the anode. (Evidence for such evolution stemmed from high acidity levels of the solution in the neighbourhood of the anode in comparison with the neutral pH values of the bulk solution.) The inferred hydrogen ion activity and a consequent reaction with the solid anodic film of TiO_2 is thought to have eventually caused a breakdown of this film. ECM is proposed to take place then by localised attack at active sites on the anode.

Tungsten carbide is another example in which passivation hinders machining. The cobalt in this metal forms a passive oxide film which has to be broken if machining is to be achieved. Although sodium nitrate is known to dissolve the basic tungsten carbide metal, the addition of an aggressive anion is helpful in breaking down the passive film formed by the cobalt.

Partial passivation, characterised by a thick, tenacious black film on the anode surface, is thought to be the cause of the coarse finish (surface roughness in excess of $5.2 \mu m$ CLA) and low current efficiency (about 40%) obtained with cast iron machined in 20% (w/w) NaCl at current densities from about 7.7 to $15.5 A/cm^2$ [18], flow-rates in the range 0.4 to $1.4 \times 10^{-3} m^3/s$ being used.

Normalised, and quenched and tempered steels, with carbon contents of 0.99% and 1.26%, machined in 20% (w/w) NaCl at $25 A/cm^2$ and 15 V, have also yielded low current efficiencies and dull granular

finishes [16]. The performance of these metals appears to be influenced by a slightly soluble resistance layer which favours partial passivation. (The values of the other process variables in these experiments were: gap width, 0.75 mm; inlet temperature, 18 to $27^\circ C$; electrolyte velocity, 16.5, 27, and $45 m/s$).

4.5.5 Transpassivation

On further increase in potential, conditions at an anode may change from the passive to the transpassive state. In the polarisation curves, this change is seen as a marked increase in current density [along line DE in Fig. 4.6(c)]. It is caused by the anodic oxidation of the original, slightly soluble passive oxide film to a soluble form. With the occurrence of transpassivity efficient ECM takes place. A good example is provided from the work by LaBoda and McMillan [19] on the ECM of low-alloy nickel-chromium steel in 450 g/l $NaClO_3$ solution. Using current densities of 39 to $116 A/cm^2$ and a (maximum) flow-rate of $0.63 \times 10^{-3} m^3/s$, they achieved surface finishes of $0.1 \mu m$. Later work established that these experiments must have been conducted in the transpassive region.

4.5.6 Transition from active to transpassive dissolution

Transpassive machining conditions can also be reached from an initial, active state of dissolution. Then, the transition becomes evident by the change from a dull, etched finish to a smooth, bright

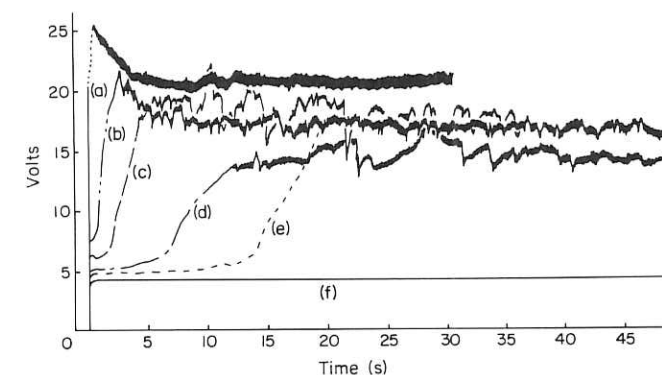


Fig. 4.9 Cell voltage transients measured in 2N KNO_3 with flow-rate $0.3 m/s$; current density (A/cm^2): (a) 16.5, (b) 8.3, (c) 5.6, (d) 4.4, (e) 4.0, (f) 3.4 (after Kinoshita et al. [3]).

one. Transient cell voltage-current measurements can also reveal this transition. Figure 4.9 shows such behaviour for galvanostatic dissolution of copper in 2N KNO₃ [3].

At the current density of 3.4 A/cm², the metal dissolves indefinitely in the active mode. At a higher current density and after a transition time with active dissolution, the dissolution process changes to the transpassive mode. The cell voltage is then about 10 to 20 V higher than that for the active mode. The critical current density at which this change occurs is increased by increased flow-rate, the transition period being shortened by increased current density and decreased flow-rate. Figure 4.9 also shows that voltage fluctuations occur in the transpassive mode.

Since the transition from active to transpassive dissolution is influenced by flow-rate and current density, a short digression on the possible cause of this effect is of interest [13].

First, the expression is introduced which describes the experimental mass transfer rates at small distances from the leading edge of the electrode and for fully developed velocity profiles:

$$Nu = 0.28 Re^{0.58} Sc^{1/3} \left(\frac{d_h}{L} \right)^{1/3} \quad (4.8)$$

[cf. Equation (3.33)]. Here, Nu is defined by

$$Nu = \frac{J_1 d_h}{z F C_b D} \quad (4.9)$$

in the usual notation.

Next we note that there is some indication from experiments that, at high dissolution rates, the product of the metal ion concentration and anion concentration might exceed the solubility product [cf. Chapter 3, Section 3.1(f)] [13]. The onset of this condition could lead to the precipitation of salt crystals, thereby initiating passivation.

For known hydrodynamic conditions, the Nusselt number corresponding to this condition may be calculated from Equation (4.9). Then, from Equation (4.8) and from the experimentally observed passivation current densities, J_p , an estimate can be made of the interfacial concentration of ionic dissolution product, C_s :

$$C_s = \frac{J_p d_h}{z F D N u_p} \quad (4.10)$$

Table 4.9 Calculations of interfacial concentration of copper salt at onset of transpassive dissolution (after Kinoshita et al. [3]) (Values used in calculations: $D = 5 \times 10^{-6}$ cm²/s; $v = 1$ mm²/s; $d_h (= 2h) = 1$ mm; $L = 0.53$ mm; $z = 2$; $F = 9.65 \times 10^4$ As)

Electrolyte	Electrolyte velocity (m/s)	Reynolds number	Passivation current density (A/cm ²)	Interfacial concentration (mole/l)
2N KNO ₃	0.30	510	3.8	4.5
	2.00	3 390	8.5	4.6
	6.27	10 600	31.0	8.5
1N K ₂ SO ₄	0.50	730	1.5	1.4
	2.00	2 920	4.1	2.2
	6.86	10 000	8.5	2.2
1N H ₂ SO ₄	0.50	770	3.6	3.4
	2.00	3 090	4.7	2.5
	6.86	10 600	11.8	3.0
2N KCl	0.50	820	0.4	0.8
	2.00	3 270	1.2	1.2
	6.06	10 000	2.5	1.2

where Nu_p is the Nusselt number associated with J_p . Calculated concentrations for a range of electrolytes, flow-rates, and passivation current densities are given in Table 4.9. In addition, solubilities of copper salts are presented in Table 4.10. Qualitative comparison of the two tables suggests that the onset of transpassive dissolution is approximately coincident with the limiting transport of dissolved reaction products by convective diffusion. Although similar behaviour has been known to occur in nitrate and sulphate solutions, in KCl no sharp transition from active to transpassive conditions

Table 4.10 Solubilities of copper salts (room temperature) (after Kinoshita et al. [3])

Salt	Solvent	Solubility (mole/l)
Cupric nitrate	H ₂ O	7.0
Cupric sulphate	H ₂ O	1.4
	1N H ₂ SO ₄	1.1
Cuprous chloride	2N KCl	1.0
	3N KCl	1.9

has been found. Instead, periodic voltage oscillations in the transition region have been observed. The anodic behaviour in this chloride electrolyte is thought to be much more complicated, since various complexes may be formed depending on the local chloride concentration. For example, owing to the effect of chloride concentration on the solubility of cuprous ion, the formation of precipitate layers is dependent on the rate of arrival of anions at the interface as well as on the rate at which cations depart from the interface. Consequently, the mass transport of chloride ions may also be a limiting factor. Nevertheless, calculations have shown that for copper dissolution in 3N KCl the rate-limiting concentration difference for the onset of transpassivation (3.6 mole/litre) is of the same order as the solubility of CuCl in that solution (1.9 mole/litre). It is possible that, for some conditions, passivation in chloride solutions is caused by a process of precipitation which is similar to that for sulphate and nitrate solutions.

4.5.7 Periodic phenomena

The abrupt rise in anode potential which occurs for transpassive dissolution conditions appears to be linked with a thin compact layer on the anode surface.

Further investigations of the nature of anodic layers have indicated that, while their formation is initiated by mass transport limited processes, their removal also involves other factors. For example, the removal of these layers is known to become accelerated at higher current densities and flow-rates, and the rate at which they are removed can exceed their rate of formation at lower current densities. The current density effect may have one or several causes. First, with an increase in current density, greater power dissipation probably takes place through this layer, thereby decreasing its effective resistance. The consequent resistance heating may produce stresses within the layer which lead to its periodic rupture. Alternatively, the influence of current density may be caused by higher local temperatures which increase the rates of chemical dissolution, or by the collection of larger concentrations of hydrogen ions at the surface. The effect of flow-rate may be simply related to increased mechanical removal of solid products, or to increased rate of mass transport of dissolved products.

Periodic phenomena associated with unstable surface films occur for many metal-electrolyte combinations. In potentiostat work,

these phenomena are seen as current density oscillations; in galvanostatic studies, they take the form of electrode potential fluctuations. The films may be salt films formed before the onset of passivation, or the films arising from the electropolishing process, or the films associated with transpassive dissolution.

For instance, Postlethwaite and Kell [20] have observed periodic potential fluctuations during galvanostatic anodic dissolution of iron in 20% (w/v) NaCl solution. In their experiments, Tafel behaviour was observed up to a critical current density (200 mA/cm^2) above which resistance to dissolution increased. This effect was seen as an abrupt increase in slope of the anode potential-current density curve. In this region the oscillations in potential took place. They were attributed to the presence of an unstable, porous, non-protective film, which was found to contain 70% iron.

Similar behaviour has been encountered during potentiostat work on carbon steels in 20% NaCl solution [16]. Again the oscillations appear to have been caused by the observed periodic rupture of a black film on the anode surface.

The nature of such oscillations has been studied during the galvanostatic dissolution of copper in NaClO_3 electrolyte [21]. Figure 4.10 shows the different types of potential oscillations which arise with increasing current density. Note that the period of oscillation decreases, and the shape of the cycle changes, with increasing current density. The period also has been found to increase slightly with increasing flow-rate.

Low current density studies (below 5 A/cm^2) have shown that any single period of oscillation has two characteristic phases, I and II, say. The length of phase I decreases as the current density is increased,

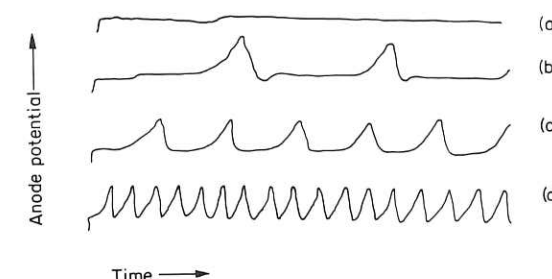


Fig. 4.10 Schematic representation of variations in form of potential oscillation: (a) $J (\text{A/cm}^2) < 0.03$; (b) $0.5 < J < 5$; (c) $5 < J < 10$; (d) $J > 10$ (after Cooper et al. [21]).

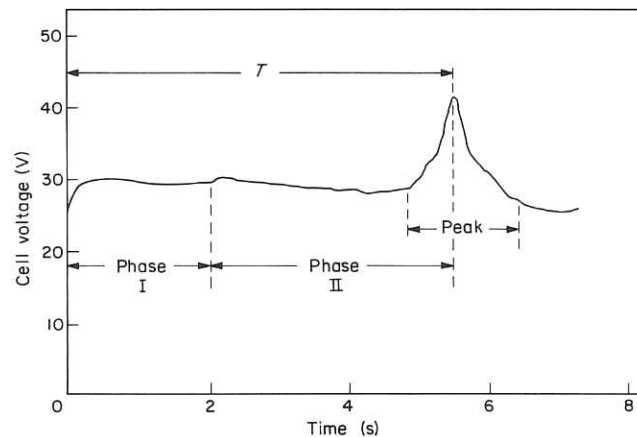
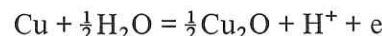


Fig. 4.11 Characteristic phases of a single period of oscillation (after Cooper et al. [21])

and becomes negligible at current densities above 5 A/cm^2 . The characteristics of the second phase are a region of low potential and a potential peak. These phases are illustrated in Fig. 4.11 for copper dissolved in unstirred 2N NaClO_3 solution at 1.33 A/cm^2 . This investigation showed that the potential cycle reflects the periodic formation and rupture of surface films. In phase I, a strongly adherent surface film of cuprous oxide was formed. In phase II the film was weakly adherent and it appeared to contain cupric chlorate and its basic salts as well as cuprous oxide. As shown in Fig. 4.12, the film thickness increases with time throughout the low and peak potential regions. Its rupture and explosion from the surface of the film substance are coincident with the sudden drop from the peak potentials.

It has been suggested that, in neutral or weakly acidic solutions and on oxide-free surfaces, phase I dissolution is linked with the formation of a porous adherent film of cuprous oxide



(The Pourbaix diagram for these conditions indicates that the product of dissolution is more likely to be cuprous oxide than divalent copper.)

The onset of phase II dissolution is associated with the formation of a thick film of basic cupric chlorate which is loosely adherent

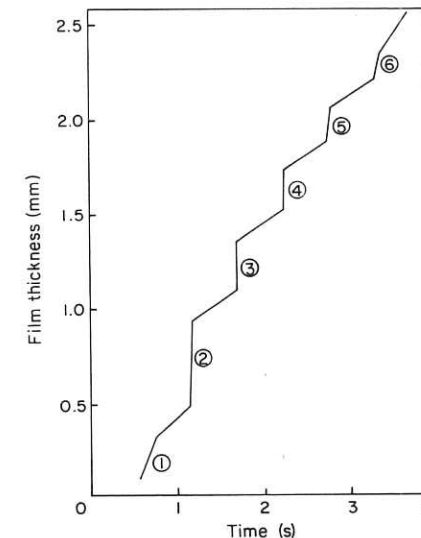
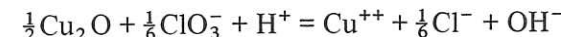


Fig. 4.12 Growth of film thickness during dissolution of copper in 3N NaClO_3 ($J = 3.12 \text{ A/cm}^2$); numbers indicate first, second, etc. potential peaks after start of ECM (after Cooper et al. [21])

to the anode surface. This process may also be related to the oxidation of Cu_2O by the chlorate ion:



Since a reaction of this type is much influenced by hydrogen ion concentration and temperature within the pores of the original Cu_2O film, the period of oscillation should be expected to increase with bulk hydrogen ion concentration, and indeed was observed in this work. (A decrease in pH should decrease the rate of growth of the films of basic salts.) The observed increase in period with flow-rate can also be explained from a greater rate of dissolution of soluble reaction products.

The potential peaks may be caused by reduced porosity of the surface film. This reduction is accelerated by the continual addition of solid products of dissolution. The dissipation of electrical power within the pore volume may then cause local vaporisation of the electrolyte. If this happens, the film should rupture and be removed. This explanation is again consistent with measurements of the highest rates of temperature increase at the anode at the onset of film breakdown.

Recently, studies have been reported on similar periodic phenomena encountered with low-carbon steel in 5M NaClO₃ [22].

4.5.8 Variation of type of finish over a machined surface

The transition from the active to transpassive modes of dissolution has been seen to be greatly influenced by the electrolyte flow-rate and current density. Variation in local conditions of flow-rate and current density can cause a consequent variation in finish over the anode surface.

For instance, suppose that upstream a metal is undergoing polishing, but that downstream some disturbance causes a local increase in

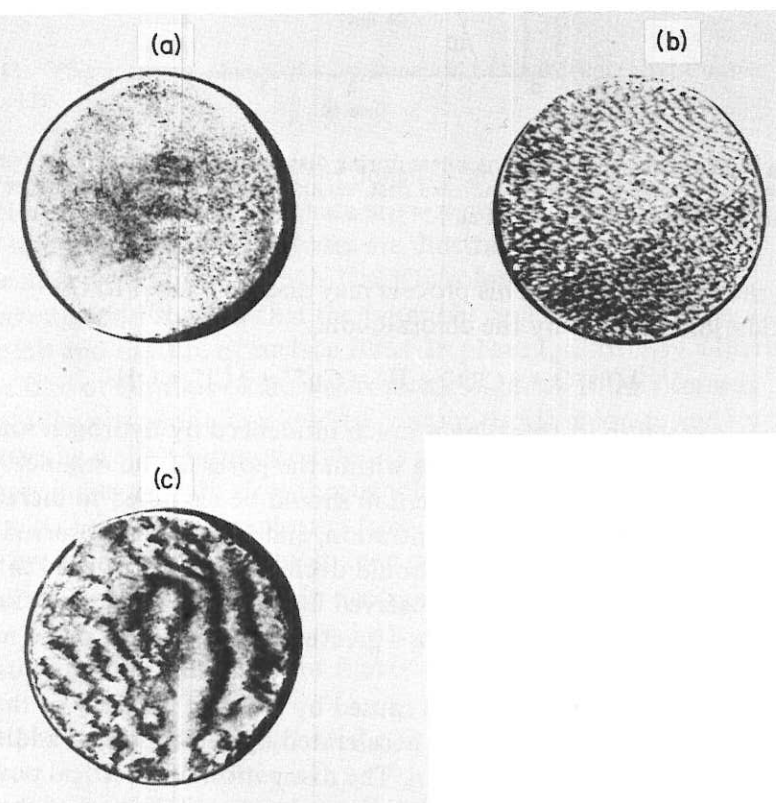


Fig. 4.13 (a) Matt, etched finish, representative of that found with nickel machined in 20% (w/w) NaCl at $35\text{ A}/\text{cm}^2$, 12 V, $0.55 \times 10^{-3}\text{ m}^3/\text{s}$, and with Monel alloy, machined at $36\text{ A}/\text{cm}^2$; (b) polished striations (Nickel machined at $58\text{ A}/\text{cm}^2$, $0.36 \times 10^{-3}\text{ m}^3/\text{s}$, 12 V); (c) selective dissolution (Monel machined at $12\text{ A}/\text{cm}^2$)

electrolyte velocity. Over the latter region, an etched surface could be obtained. Alternatively, local variations in velocity could result in intermittent changes from etching to polishing or partial passivation conditions. The extent of surface striations so produced can be diminished by a change in flow-rate so that ECM is controlled by a single process over the whole surface.

Surface variations of this nature are often encountered. In one study [5] on nickel machined in HCl solution an etched surface finish without flow marks was obtained at $7.8\text{ A}/\text{cm}^2$ and 2 V, the Reynolds number being 4700 (flow-rate $0.06 \times 10^{-3}\text{ m}^3/\text{s}$; gap width 0.25 mm). However, at $18.6\text{ A}/\text{cm}^2$ and 4 V the etched surface also bore polished patches with flow streamlines. In this case, ECM must have occurred in the transition region between the active and polishing modes of dissolution. For higher current densities, 34 and $64\text{ A}/\text{cm}^2$, and 8 V and 12 V respectively, polished finishes were obtained, although flow marks were still also evident.

In Section 4.5.4, partial passivation was described as a characteristic of some carbon steels which had undergone various heat treatments [16]. In that work, some specimens were also found to have a variation in finish over their surface. For example, 0.78% C quenched and tempered steel had the marks of partial passivation at an electrolyte velocity of 16.5 m/s but this passivation broke down as the velocity was increased to 27 and 45 m/s, and the surface then carried polished striations. These are thought to be due to local variations in flow over the anode surface causing fluctuations between conditions favourable to partial passivity and to polishing. In other cases, the fluctuations led to variations between etching and partial passivation, and etching and polishing.

These results are similar to those found in ECM experiments on nickel in 20% (w/w) NaCl. Figure 4.13 shows a matt etched finish obtained at $35\text{ A}/\text{cm}^2$, whilst at $58\text{ A}/\text{cm}^2$ the finish is polished but 'broken'.

4.6 Surface films and dimensional control

The studies described in the preceding section emphasise the close link which exists between surface finish and anodic films in ECM. The link also extends to another important aspect called *dimensional control*.

4.6.1 Dimensional control

This feature of an electrolyte can be explained by reference to Fig. 4.14 which shows an electrode configuration consisting of an initially plane anode ABCD and a cathode of simple shape PQRSTU.

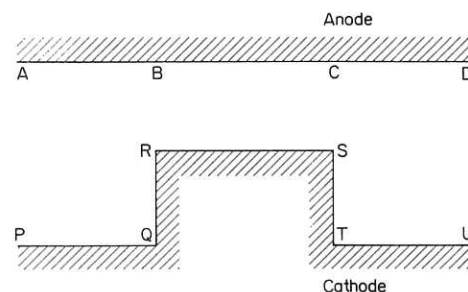


Fig. 4.14 Demonstration of dimensional control; plane anode and cathode of simple shape

Suppose that only the passage of current between RS and BC is required. In addition, however, stray current will pass from RS to the regions BA and CD, its density becoming less in the directions B to A and C to D. If surface polishing is sought along BC, the conditions of lower local current density along BA and CD may lead to etching and pitting in those regions.

The extent to which current strays in this fashion is related to the *throwing power* of the electrolyte. The corresponding problem is well known in electrodeposition. In that process, the ability of an electrolyte to provide a deposit of uniform thickness over an electrode is measured in terms of its throwing power; 100% throwing power produces a deposit of uniform thickness. In ECM, stray current is reduced at low values of throwing power; when the latter quantity approaches $-\infty$, stray current should be eliminated.

Several methods for measurement of the throwing power of solutions under ECM conditions have been reported. Brook and Iqpal [23] have modified the Haring-Blum cell which is normally used for deposition work. They have also adapted for ECM the empirical formula employed in electrodeposition for measurements of throwing power, T :

$$T = \left(\frac{L - M}{L + M - 2} \right) \times 100 \quad (4.11)$$

Here L is the 'linear ratio' of the distances of equipotential plane parallel anodes from the cathode; M is the 'metal distribution ratio' of the weight of metal dissolved from the nearer anode to the weight dissolved from the farther anode. In their experiments, two plane

Table 4.11 Throwing powers of NaClO_3 and NaCl electrolytes at 25°C (after Brook and Iqpal [23])

Electrolyte	Gap width	
	0.125 mm	0.25 mm
5% NaClO_3	-13	7
	-21	6
		3
5% NaCl	26	19
	11	12
$5\% \text{NaCl} + 0.12\% \text{K}_2\text{Cr}_2\text{O}_7$	-25	
	-22	
$\text{NaCl} + 1\% \text{BTZ}$	-17	
	-15	

anodes made of 18/8 stainless steel were placed on either side of a plane copper cathode. The linear ratio was usually maintained at 5 : 1. The smaller electrode gap width was either 0.125 mm or 0.25 mm. The current density was maintained at 2.3 A/cm^2 and the flow-rate at $0.01 \times 10^{-3} \text{ m}^3/\text{s}$. The results presented in Table 4.11 demonstrate that NaClO_3 has a lower throwing power than NaCl . To test the hypothesis that the low throwing power of NaClO_3 is linked to passivation of the anode in local current density regions, two passivation agents, benztriazole and potassium dichromate, were added to the NaCl solution. Table 4.11 shows that with these additives the throwing power of NaCl is markedly decreased. Its dimensional control is thereby improved.

An alternative method for measuring throwing power in ECM (at current densities about 95 A/cm^2) has been proposed by Chin and Wallace [24]. Their technique consists of measuring the electrode gap width as a function of machining time and expressing the linear

ratio, L , and the metal distribution ratio, M , in terms of the gap width and cutting rate respectively:

$$L = \frac{h(t)}{h(0)} \quad \text{and} \quad M = \left(\frac{dh}{dt} \right)_0 / \left(\frac{dh}{dt} \right) \quad (4.12)$$

Here $h(t)$ is the gap width at time t , and $h(0)$ is the initial width; dh/dt is the rate of change of gap width with time, the subscript denoting the initial rate. They assume a logarithmic relationship between M and L , $M = L^{1/A}$, where A is the logarithmic throwing index which is constant for a given electrolyte at constant values of the process variables. For plane parallel electrodes, they deduce an equation which describes the variation with time of the machining gap:

$$t = \frac{h(0)(L^{1/A} - 1)}{\left(\frac{dh}{dt} \right)_0 \left(1 + \frac{1}{A} \right)} \quad (4.13)$$

Measurements of gap width as a function of machining time now yield that $t \propto L^n$; e.g. $n = 1.9$ so that $A = 1/(1.9 - 1) = 1.11$. For a given linear ratio, L , the metal distribution M can now be calculated from $M = L^{1/A}$. A log-log plot of M against L should now give a straight line which passes through a common point represented by the linear ratio equal to 1, and by the metal distribution ratio equal to 1.

Landolt [25] has investigated the difference in throwing power between a non-passivating (acidified 1M NaCl) and a passivating (neutral 1M NaClO₃) electrolyte used for the ECM of nickel. His work again demonstrates that a non-passivating electrolyte has a throwing power of almost zero whilst a passivating electrolyte takes negative values.

However, little can be gained from quantitative measurements of throwing powers apart from a comparison of the performance of different electrolytes. Since calculations of this type depend on the electrode configuration and on the process variables, they reveal little information about the processes that control this property of electrolytes.

The marked difference in throwing power between a passivating electrolyte, e.g. NaClO₃, and a non-passivating one, e.g. NaCl, does not seem to be due to any characteristic effect that these types of solution might have on the current distribution within the machining

region. Such effects will be discussed in Chapters 5 and 6. A measure of their influence will be given there in terms of a dimensionless parameter, given by the product of the electrolyte conductivity and the slope of the voltage-current density curve, divided by a typical length, e.g. the gap width. The disparity in results between a passivating and a non-passivating electrolyte may be caused by a different dependence upon current density of the current efficiency for dissolution. In Landolt's studies of throwing power, for instance, the current efficiency for dissolution of nickel in NaCl solution was not influenced by current density, whilst that in NaClO₃ was strongly dependent on both current density and flow-rate. Nonetheless, much remains to be done to establish the real nature of throwing power in ECM.

4.6.2 The nature of surface films in different electrolytes

Since the quality of surface finish and dimensional control are closely associated with surface films, this section is devoted to a study of the nature of the anodic films formed in different electrolytes.

Much consideration has been given to the superior ECM results obtained with NaClO₃ solution compared with those found with NaCl electrolyte. By means of the polarisation curves shown in

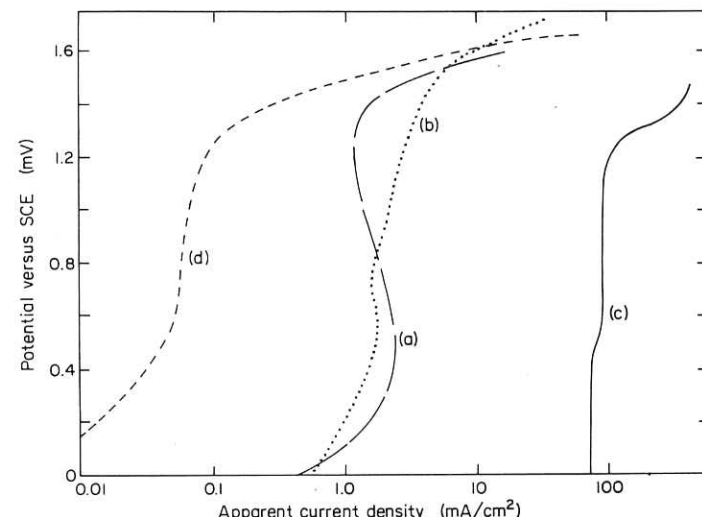


Fig. 4.15 Polarisation curves for iron; (a) NaClO₃; (b) NaNO₃; (c) NaCl; (d) Na₂Cr₂O₇ (after Hoare et al. [26])

Fig. 4.15, the performance of iron in those electrolytes and in NaNO_3 solution is first discussed [26].

In relating these polarisation curves to ECM conditions, we shall look for the range of anode potentials over which dissolution is possible, bearing in mind that in ECM the IR drop between the electrodes takes large values for small inter-electrode gap widths. If the IR drop becomes sufficiently large, the potential at the anode may decrease so much that dissolution ceases (see Chapter 3).

(a) NaClO_3 electrolyte

For NaClO_3 , active dissolution occurs at the lowest potentials; the iron dissolves as Fe^{++} ions which can be oxidised by dissolved oxygen to Fe^{+++} ions. As the potential is increased to more noble values, a critical current value is reached at which the anode surface becomes covered with a film. Further studies [27, 28] have shown that this film is $\gamma\text{-Fe}_2\text{O}_3$ and that its thickness is about 10^{-7} m. As the film forms over the active sites on the metal, dissolution is inhibited by the onset of passivation with corresponding reduction in current. On further increases in the potential, the film is broken down, and the transpassive region of dissolution is reached with an equivalent increase in current. ECM is assumed to occur in this region.

Figure 4.15 shows that with NaClO_3 solution the transition from passive to transpassive conditions is abrupt. Accordingly, the potential range between dissolution and non-dissolution is very narrow. Hence, in a shaping operation with NaClO_3 electrolyte, ECM should occur mainly in the region of smallest gap, with little ECM taking place outside that region. Good dimensional control is then achieved.

(b) NaNO_3 electrolyte

For NaNO_3 , the transition from passivity to transpassivity is less sharp than that for NaClO_3 . ECM over a wider region on the anode can therefore be expected. Since the transpassive region also lies at a more noble potential for NaNO_3 than for NaClO_3 , the machining rate at the same operating conditions for NaNO_3 solution should be less than that for NaClO_3 . This observation has been confirmed by ECM experiments in which the current efficiencies for metal removal and oxygen generation are about 12% and 85% respectively [29]. These processes appear to be influenced by the formation of a film of Fe_3O_4 on the anode surface. The film also seems to be

electronically conducting and to favour a chemical reaction other than metal dissolution.

Since the thickness of this film is not noticeably decreased in the transpassive region, the surface finish is not likely to have the brightness expected when a thinner compact film, commonly associated with electropolishing, is present. ECM experiments again bear out this suggestion; reported typical surface roughnesses in 3M NaNO_3 are about 0.65 to 1 μm RMS.

(c) NaCl electrolyte

For NaCl , the current density in the polarisation curve is seen to be much higher than that for the other electrolytes. Dissolution is then possible at even the lowest potentials. Consequently, in ECM, dissolution will still occur even at very wide gaps, resulting in considerable stray machining and poor dimensional control. These machining conditions are probably due to an iron salt on the anode surface, whose presence prevents the metal changing from its active state. The film appears to be a thick, unprotective layer of porous salts, e.g. Fe(OH)_2 [28].

(d) $\text{Na}_2\text{Cr}_2\text{O}_7$ electrolyte

Since dimensional control with NaNO_3 electrolyte is better than that with NaCl , but poorer than NaClO_3 , it has been suggested that the presence of an anion which contains oxygen may be necessary if stray current is to be diminished. This premise has led to a survey of chromate electrolytes, since a protective film of $\gamma\text{-Fe}_2\text{O}_3$ is known to form on iron in these electrolytes. From Fig. 4.15, the polarisation curve for $\text{Na}_2\text{Cr}_2\text{O}_7$ solution indicates the presence of a strongly passivating film. Although this film is removed abruptly in the transpassive region, the potentials then are much higher than for NaClO_3 . In ECM, electrical sparking becomes likely. Indeed, poor ECM results have been obtained with $\text{Na}_2\text{Cr}_2\text{O}_7$ solutions, and with other passivating electrolytes, Na_2CO_3 and Na_3PO_4 , no machining has been possible. Polarisation and ECM experiments with steel in NaClO_4 and Na_2SO_4 electrolytes and mixtures of them have also shown that these electrolytes are inferior to NaClO_3 [30]. NaClO_3 electrolytes appear to be unique in ECM in that the transition from the passive to the transpassive region is a sharp one; also, the latter regions occupy potentials which are the least noble.

On this basis, it has been suggested that good dimensional control requires (i) the formation of an anodic passivation film, and (ii) the occurrence over a narrow band of potentials of the transition from passivity to transpassivity [27]. This view, however, is not universally held. Landolt contends that the width of the passive potential region in a potentiostat current-potential curve should bear little influence on current distribution in ECM [25]. The basis for this claim is that the polarisation parameter, which dictates the extent to which current distribution in ECM is affected by an electrolyte's throwing power, depends only on the slope of the current-voltage curve, and not on actual values of the anode potential.

Although the merits of NaClO_3 are undoubtedly similar dimensional control has also been claimed to be possible with simple NaCl solutions [31, 32]. The reasoning behind this claim can be clarified from the anode potential-anion concentration diagram, Fig. 4.16. This diagram shows the likely surface finish produced for particular conditions of potential and concentration. Suppose that machining is performed in a region where the conditions are given by A. The surface finish then achieved should be bright and polished. In a neighbouring zone which is at lower potentials, B, passivity will occur. If chloride ions are present, they are likely to attack the passive film causing pits to

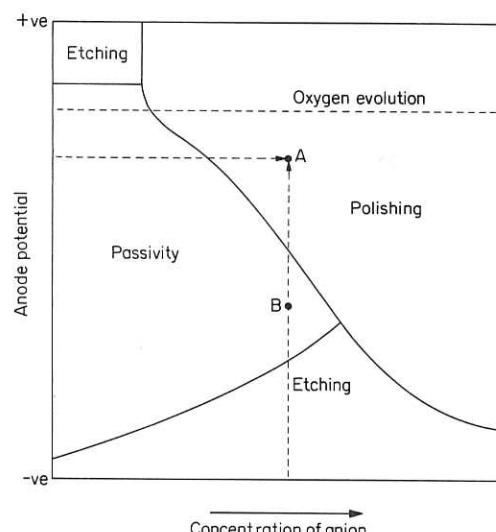


Fig. 4.16 Influence of anion concentration and anode potential upon surface finish (after Boden and Evans [32])

form. On the other hand, the presence of chlorate ions should produce only a mild attack. Clearly, the ability of the passive film to resist anion attack is critical if stray current is to be diminished. But even if a passive film is formed, its efficacy can be spoiled by severe pitting in the passive (stray current) region; also the problem of choice of a suitable additive becomes aggravated by the need to reduce the depth and number of pits in the stray-current zone without affecting machining in the main region, A.

Suitable solutions appear to be those which form insoluble salts, e.g. with nickel anodes, a combination of NaCl with Na_2CO_3 forms insoluble nickel carbonate. Combinations of solutions which produce soluble salts behave like NaCl , e.g. NaCl with Na_2SO_4 . For nickel machined at a flow-rate of 30 m/s and a maximum current density of 15.5 A/cm^2 in 15% (w/w) NaCl containing 2.5% (w/w) Na_2CO_3 , the amount of pitting was found to be considerably less than that of the simple 15% NaCl solution; indeed, the performance of the former solution almost matched that of a 40% NaClO_3 electrolyte. In contrast, a solution of 15% $\text{NaCl} + 1\%$ Na_2SO_4 gave only a slight reduction in pitting owing to the formation of a relatively soluble nickel sulphate salt.

The improvement gained with insoluble nickel salts appears to be due to the precipitation of these salts around the pits in the stray current region. But success also depends critically on the quantity of anion addition to the basic sodium chloride electrolyte. For instance, in the ECM experiment above, precipitation only occurred in the stray current zone provided that the percentage of sodium carbonate in the 15% NaCl solution was below 2.5. Brightly machined surfaces with high current efficiencies could then be achieved in the main machining zone. But at higher concentrations of Na_2CO_3 , precipitation also occurred in the main zone with the onset of passivation, that is, coverage of the surface with insoluble nickel carbonate and a reduction in machining rate.

These observations indicate that the ECM of iron or steel in NaClO_3 is quite different from that of nickel in this electrolyte. This has been confirmed in tests on nickel machined in a solution of 350 g/l NaClO_3 [33]. Some results are summarised in Table 4.12. They show that the current efficiency for nickel removal does not increase as rapidly with current density as it does for mild steel, nor does it achieve as high values. It was also found that, under identical operating conditions, the maximum machining rate for

Table 4.12 Current efficiency values for steel (type 1020-U.S.) and nickel (99.5% pure) machined in 350 g/l NaClO₃ solution (after LaBoda et al. [33])

Metal	Current density (A/cm ²)	Current efficiency (metal removal) (%)	Current efficiency (O ₂ generation) (%)
Steel	40	0.3	—
	80	22	78
	150	62	40
	300	86	18
Nickel	40	8	—
	80	15	79
	150	58	—
	300	67	40

nickel was about one-half of that for mild steel (0.07 mm/s and 0.13 mm/s respectively). Corresponding roughness measurements also showed a contrast: 0.26 to 0.39 µm for nickel against 0.026 to 0.052 µm for steel. These results are consistent with polarisation experiments which show that, with increasing potentials, the anodic film on nickel thickens, unlike the film on mild steel which under similar conditions becomes uniformly thinner and favourable towards electropolishing conditions.

This work again establishes that the performance of a metal in ECM varies from one electrolyte to another and depends greatly upon the nature of the anodic films which are formed and upon their interaction with the anions in the electrolyte.

4.7 Surface finish: some macroscopic effects

4.7.1 Selective dissolution with alloys

When a metal has constituents whose electrode potentials are different, those with the lowest potential will first be dissolved. At low current densities, the result at the surface of the metal is differential dissolution of the constituents, observable as a variation in surface

finish. At higher current densities, the effect of differences in electrode potentials of constituents is reduced, since the applied potential difference at the anode is then higher, and the potentials required for dissolution of the constituents are more easily achieved.

A similar effect can be found with a metal whose surface includes a grain of different electrode potential from that of the surrounding material. If the electrode potential of the grain material is greater, then its dissolution will not occur until the potential at the anode surface reaches its electrode potential. During that time, the surrounding material will be machined, leaving the grain protruding at the surface. On the other hand, if the grain has a lower electrode potential, its dissolution will proceed first, leaving a recess on the surface. This effect is often observed as grain boundary attack. Owing to the traction forces created by the high rates of electrolyte flow in ECM, grains can even be dragged from the metal surface; increased surface roughness is then observed.

Photographs of Monel alloy machined in 20% (w/w) NaCl solution are presented in Fig. 4.13 to illustrate selective dissolution. At 12 A/cm², the copper (dark lines) is separated from the nickel constituents (light lines). At the higher current density, 36 A/cm², the effect is less obvious, the surface being smoother and more uniform.

Attack along the grain boundaries of Nimonic 80A dissolved in 0.1M to 4.3M NaCl has been the subject of a detailed study by Evans and Boden [34]. They found that the severity of grain boundary attack could be lessened by a decrease in electrolyte flow-rate, from about 30 to 6 m/s, the maximum current density being about 1.5 mA/cm². They postulate that, because of the high rates of dissolution along the grain boundary regions, conditions favourable to polishing should first be achieved. But for the high rates of metal removal to be maintained there, the process of dissolution becomes greatly dependent on the rate of arrival of water molecules. At lower electrolyte flow-rates, this rate of arrival will be decreased. Salt passivation then arises, and with it a reduction in the amount of grain boundary attack.

4.7.2 Flow separation

An anode surface, which initially is irregular, may also cause flow separation between the 'hills' and the 'valleys' on its surface. At this stage, a short discussion on the possible effects of flow separation is useful, particularly since it reinforces the explanations given in

Section 4.5.8 for the variations of finish over the surface, which are so often observed.

The basis of the argument is that, over a flat anode, the diffusion layer can be assumed to be adjacent to the surface. Metal removal is controlled by the usual diffusion-migration mechanism, discussed

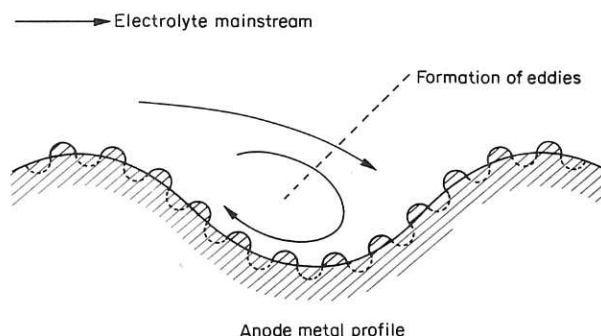


Fig. 4.17 Formation of eddies in 'valley' of anode metal

in Chapter 3, and because of the high electrolyte velocity, concentration polarisation can be assumed to be negligible. But the flow over an irregular anode could be quite different. Around the hills, the flow still adheres to the metal surface. Metal removal continues to be governed by the processes outlined above. On the dissolution of both large and small scale irregularities, the result should be a polished surface in that region. In the valleys, a different situation arises, as suggested in Fig. 4.17. Here the flow separates from the metal surface, causing a rotating eddy in the region between the mainstream of the electrolyte and the metal surface in which a large uniform concentration of metal ions may be built up. This may cause a high concentration overpotential in that region, making difficult the local removal of the smallest irregularities. Polishing is not then achieved, and a matt, etched finish can be expected. This could explain the type of 'broken' polished finish, observed by Cuthbertson and Turner [6]. If the pre-machining preparation of the anode surface, carried out by them to remove an oxide film, also involved some smoothing of the surface, this, of course, would also reduce the initial heights of surface irregularities, causing a more uniform flow pattern. This, in turn, would reduce the probability of eddies, and overall polishing would again be more likely.

Freer, Hanley, and MacLellan [16] have also suggested that observed unevenness and striations, superimposed on surfaces after ECM, could be caused by local variations in flow. If the flow conditions lead to electropolishing (diffusion control) over the hills, the lower rates of flow in the valleys may cause etching (activation control) in those regions. Local variations in rate of flow may also account for surface unevenness due to fluctuations between conditions favourable to partial passivation and either activation or diffusion control. Partial passivation will lead to a locally raised region (due to reduction in machining rate) protruding over the regions where activation or diffusion mechanisms have caused the rate of dissolution to be greater. Sufficiently high rates of flow can reduce the extent of all these effects.

Non-uniform flow can also arise from cavitation phenomena. Even if their effect is not sufficiently great to cause a short-circuit, the variation in the flow pattern usually becomes apparent by striations developed on the anode surface.

4.7.3 Hydrogen gas

As the electrolyte flows downstream within the machining gap, it collects in solution an increasing amount of the hydrogen gas generated at the cathode. The presence of the gas-electrolyte mixture has diverse effects on the ECM process, many of which will be discussed in Chapter 5. But a principal effect can be appropriately introduced here, namely, a decrease in effective conductivity of the solution. This decrease becomes more marked in the downstream direction, and has a consequential influence on surface finish.

Further observations from the work above [32] become relevant. In that study, plane parallel electrodes, spaced 0.25 mm apart, were used; the flow-rate was 30 m/s and the current density 15.5 A/cm². Polishing of the nickel anode was sought over the central machining region. At the same time, attempts were made to reduce the depth and number of pits in the passive, stray current zone situated upstream and downstream. The extent of stray current attack was found, in fact, to be diminished by a reduction in the concentration of the NaCl solution, e.g. from 20 to 13.5%. But in the downstream, stray current zone, a further decrease in pitting was achieved. This was attributed to a decrease in the effective conductivity of the solution by the accumulation of hydrogen gas bubbles. But the addition of small quantities of Na₂SO₄ (1%) and Na₂CO₃ (2.5%)

to a main 15% (w/w) NaCl electrolyte led to increased pitting in these areas, mainly because these mixtures of electrolytes have a higher conductivity and are therefore less affected by the hydrogen gas.

The specimens used in this study were ground and mechanically polished so that they had a perfectly flat surface before ECM. In practice, however, some previous machining or working operation could make the anode surface slightly irregular before its treatment by ECM. For a surface of this initial form, a theoretical investigation is available which deals with the effects of hydrogen gas on the eventual finish achieved by ECM [35]. The bases of that study are considered in detail in Chapter 6, since they also cover the problem of anodic shaping in its simplest form, anodic smoothing. But those features relevant to the present study can be introduced here.

Suppose now that the anode surface is not initially flat, but that it consists of a series of irregularities of widely varying horizontal and vertical dimensions. Smoothing is achieved by the non-uniform dissolution of the anode surface, the peaks being dissolved faster than the valleys. The removal of the smallest irregularities constitutes 'polishing' or 'brightening'.

The theory of anodic smoothing (Chapter 6) predicts that for a flat surfaced cathode and an anode with a sinusoidal irregularity of wavelength λ ($= 2\pi/k$, where k is the wave number) and amplitude ϵ which is small compared with the average gap width p , the irregularity is reduced at a rate given by

$$\epsilon(t) = \epsilon(0) \exp\left(-\frac{MVk \coth kp}{p}t\right) \quad (4.14)$$

where $\epsilon(0)$ is the initial amplitude, M a machining parameter ($= e_a \kappa_e / \rho_a$), e_a being the electrochemical equivalent of the metal and ρ_a its density, and κ_e the electrolyte conductivity, V the applied potential difference, and t the machining time. This formula is valid provided that the gap width is maintained at its steady-state value,

$$p_e = \frac{MV}{f} \quad (4.15)$$

determined from the equation, proved in Chapter 6,

$$\frac{dp}{dt} = \frac{MV}{p} - f \quad (4.16)$$

where f is the cathode feed velocity.

The result (4.14) demonstrates that short-wavelength irregularities are removed more rapidly than those of longer wavelength. We shall see in Chapter 6 that Fourier analysis may be used to extend these results to describe the behaviour of an irregularity of arbitrary profile. Clearly, sharp-profile irregularities are removed more rapidly than 'bluff' ones, and the irregularities are reduced to a sinusoidal form of basic wavelength. Local polishing, as distinct from long-wavelength smoothing, occurs comparatively quickly; an overall polished surface may be obtained with low amplitude, long-wavelength irregularities. This difficulty is enhanced by the increase of the machining rate (i.e. increase of current density, or of the factor MV in Equation (4.14)).

The theory also applies to cases where the electrodes may be considered to be locally plane and parallel, i.e. if the radius of curvature of the electrode configuration is large compared with the gap width.

Variations in the surface finish due to the electrolyte flow may be explained further in terms of changes in the effective conductivity of the electrolyte. As we shall see in Chapter 5, the conductivity will be affected by factors such as electrolyte heating and hydrogen gas bubble generation. Joule heating will increase the temperature and so increase the conductivity, whilst hydrogen gas will reduce it by decreasing the volume of electrolyte available for conduction. Both effects are cumulative in the downstream direction of the electrolyte flow. Under steady-state machining conditions, these changes in conductivity are compensated by a corresponding change in the inter-electrode gap width, so that the steady-state current density does not vary locally along the electrode length. However, if such equilibrium is not achieved in the machining time required for electrochemical smoothing to a certain degree, then local variations in conductivity along the electrode length, and hence in current density and in surface finish, might therefore be expected. The following analysis has been proposed to explain these related effects of gas and flow on surface finish.

It will be recalled that Equation (4.14) for the removal of the irregularities involves a machining parameter, M , which depends directly on conductivity. If, in this simplified analysis, overpotential effects are excluded, conductivity is the only factor in the equations for smoothing which is dependent on conditions in the electrolyte. To examine its effects, we replace κ_e in Equation (4.14) by κ_m , a mean effective conductivity.

For simplicity, the gap is assumed to remain constant at its mean value p , and variations in current density and conductivity along the electrode length are sought (cf. the actual, steady-state situation where the current density is constant and the gap width varies). The mean conductivity κ_m along the gap may be expressed in terms of the conductivities in the electrolyte zone free of bubbles and the bubble layer:

$$\kappa_m = \kappa_e \exp\left(-\frac{1.5 \kappa_e H_g V}{U p^2} x\right) \quad (4.17)$$

where κ_e is the electrolyte conductivity in the gap zone which is free of hydrogen bubbles, H_g is the volume of hydrogen produced per coulomb, U is the electrolyte velocity, assumed constant, and x is the distance downstream. The derivation of this equation is rather lengthy; it depends on the experimentally observed results that the bubble layer thickness increases linearly along the gap [36], and that for a two-phase mixture the ratio of the conductivity in the bubble zone to the conductivity outside the zone is equal to $(1 + \alpha)^{-1.5}$, where α is the void fraction [37]. Nonetheless, the full analysis is readily available [35].

Since the machining parameter M and the conductivity have the same dependence on distance x , then qualitatively the modified expressions for κ_m and M mean that their values decrease in the

Table 4.13 Effects of electrolyte velocity, U , and distance along the electrode, x , on the ratio $\epsilon(t)/\epsilon(0)$

Long wavelengths

	$x = 10$ mm			$x = 50$ mm			$x = 100$ mm		
U (m/s)	1	10	20	1	10	20	1	10	20
$\epsilon(t)/\epsilon(0)$	0.85	0.56	0.53	1	0.72	0.62	1	0.85	0.72

Short wavelengths

	$x = 10$ mm			$x = 50$ mm			$x = 100$ mm		
U (m/s)	1	10	20	1	10	20	1	10	20
$\epsilon(t)/\epsilon(0)$	0.19	0	0	1	0.04	0.01	1	0.19	0.04

downstream direction, or if the electrolyte velocity is decreased. If these reduced values for M are substituted in the earlier equations for $\epsilon(t)$, the conclusions are that surface roughness increases in the direction of flow and that the overall roughness decreases if the electrolyte velocity is increased.

Results of some calculations are presented in Table 4.13. They have been obtained by the substitution in Equation (4.17) of the typical values, $\kappa_e = 0.2 \text{ ohm}^{-1} \text{ cm}^{-1}$, $H_g = 0.12 \times 10^{-6} \text{ m}^3 \text{ A}^{-1} \text{ s}^{-1}$, $p = 0.5 \text{ mm}$, $U = 1, 10, 20 \text{ m/s}$, $x = 10, 50, 10^2 \text{ mm}$, $V = 10 \text{ V}$, $t = 10 \text{ s}$. From the calculated values of κ_m , modified values for $M (= 8.5 \times 10^{-5} \kappa_m)$ have been found. These values have been used in Equation (4.14) for $\epsilon(t)/\epsilon(0)$, in which a value $k = 20 \text{ mm}^{-1}$ has been taken. Note that in Table 4.13 two cases have been considered: one in which the irregularities are of long wavelength ($kp \ll 1$), and another in which the wavelengths are short ($kp \gg 1$). For the former case, Equation (4.14) reduces to

$$\frac{\epsilon(t)}{\epsilon(0)} = \exp\left(-\frac{MV}{p^2} t\right) \quad (4.18)$$

whilst, for the latter condition,

$$\frac{\epsilon(t)}{\epsilon(0)} = \exp\left(-\frac{M V k}{p} t\right) \quad (4.19)$$

Experimental results of this type have been obtained in work on Nimonic 80A machined in saturated NaCl solution [6]. In that study, specimens were machined in the same condition in which they were received, i.e. without their surfaces being mechanically treated before ECM. At a current density of 31 A/cm^2 and a flow-rate of 12 m/s , the surface roughness increased markedly in the downstream direction. An increase in velocity to 28.5 m/s had the effect of improving the quality of finish.

4.7.4 Effects of overpotential

The analysis in Chapter 6 upon which the results in Section 4.7.3 are based is of further interest in that it provides information about the effects of overpotential upon surface finish. Again, for brevity, only the main results from that chapter are presented here. As before, the cathode is considered to have a flat surface whilst the anode surface is initially irregular.

In Chapter 6, the basic theory is extended to include an arbitrary, current density-dependent overpotential. In that study this overpotential is initially supposed to exist only at the cathode. The overpotential is also assumed to cause a small departure in the value of the current density at the anode, J , from the mean current density, \bar{J} , say. The overpotential function, written here as $f(J)$, can then be expanded as a Taylor series:

$$f(J) = \alpha + \beta(J - \bar{J}) \quad (4.20)$$

where

$$\alpha = f(\bar{J}) \quad (4.21)$$

and

$$\beta = \frac{\partial f}{\partial J} \Big|_{J=\bar{J}} \quad (4.22)$$

Then, as shown in Chapter 6, Equation (4.14) takes the modified form

$$\epsilon(t) = \epsilon(0) \exp \left[-\omega M \left(\frac{V - \alpha}{p} \right) kt \coth kp \right] \quad (4.23)$$

where

$$\omega = 1 - \beta \kappa_e k \operatorname{cosech} kp \operatorname{sech} kp (1 + \beta \kappa_e \coth kp)^{-1} \quad (4.24)$$

Note that the quantity $\beta \kappa_e$ has the dimension of length. It is equivalent to the electrodeposition polarisation parameter, discussed by Wagner [38], which is given by the product of the electrolyte conductivity and the slope of the voltage-current density curve of the electrolytic cell.

Two particular cases can now be considered. For short-wavelength irregularities, $kp \gg 1$; ω is negligibly different from unity. The dissolution of such irregularities is unaffected by overpotentials.

For longer wavelengths,

$$\omega \approx \left(1 + \frac{\beta \kappa_e}{p} \right)^{-1} \quad (4.25)$$

That is, for large values of the dimensionless parameter, $\beta \kappa_e / p$, the rate of dissolution is zero. The overpotential also has an effect on the equilibrium gap, the expression for which becomes

$$p = \frac{M(V - \alpha)}{f} \quad (4.26)$$

The cathode overpotential, therefore, has the following principal effects:

- (i) decrease of the mean machining rate;
- (ii) decrease of the removal rate of surface irregularities of long wavelength.

An analogous discussion of anode overpotentials shows that the behaviour of long-wavelength irregularities is similar to the cathode overpotential case; for very high values of the overpotential parameter $\beta \kappa_e k$, however, the reduction rate of all irregularities is very small, irrespective of the wavelength. Smoothing is then very difficult, the initial, irregular anode profile being 'frozen' as machining proceeds.

4.8 Use of molten salt electrolytes

The electrolytes studied so far have been restricted to aqueous types. It will have become obvious, too, that the rates of reactions in ECM can usefully be increased by operation at high electrolyte conductivities and temperatures. Because aqueous electrolytes have their limitations (e.g. those due to their boiling temperatures) some attention has been paid to the possible use of molten salt electrolytes in ECM. These solutions have the attraction that their values of density and viscosity are similar to those of aqueous electrolytes, whilst they have electrical conductivities which are often greater by more than an order of magnitude. For example, molten NaOH has a conductivity of $2.44 \text{ ohm}^{-1} \text{ cm}^{-1}$, a density of 1.77 g/cm^3 , and a viscosity of 3.79 cP at 630°C . As a molten electrolyte, NaOH has been used for the ECM of tungsten carbide [39]. Current densities as high as 186 A/cm^2 were achieved, in comparison with a maximum 49 A/cm^2 possible with aqueous NaCl under the same experimental conditions. The metal removal rates were correspondingly higher and a smooth uniform surface finish was obtained. This electrolyte in its molten form has been thought to be a better candidate than NaCl because of its lower melting point (about 320°C compared with 800°C for NaCl).

Lovering has studied the polarisation behaviour of nickel, Nimonic, and titanium alloys in molten KNO_3 electrolyte at 350°C [40]. He reports that *cathodic* polarisation leads to the dissolution of these metals, the apparent current efficiency being less than 10%. The anodic polarisation of titanium leads to the development of a

thick, electronically conducting film on the metal surface, with O₂ gas being evolved for applied potential differences up to 30 V. Oxygen gas is also invariably generated with Nimonic. On the other hand, anodically polarised nickel dissolves easily at low voltages (0.5 to 1 V) and without gas evolution.

Further experiments with LiCl-KCl electrolytes at 400°C have again confirmed that nickel based alloys can be dissolved at low anodic potentials. Apparent current efficiencies are often in excess of 100%, although these values can be attributed to the erosion of intermetallic particles. At higher potentials, chlorine gas evolution occurs in addition to metal removal. But LiCl-KCl electrolyte is not suitable for titanium and its alloys. In this electrolyte these metals dissolve spontaneously with simultaneous gas evolution.

A disadvantage of molten salt electrolytes is that they are difficult to handle. At present they are unlikely to replace aqueous solutions in ECM.

4.9 Effects of ECM on the mechanical properties of metals

Since conventional machining operations are known to modify the surface structure and mechanical properties of metals, the likelihood of corresponding effects occurring from ECM requires study.

First, no cases are known of hydrogen embrittlement of the anode surface, which, of course, can affect the ductility of the metal, and which is the cause of metal failure in some structures. Other tests have confirmed that ECM does not affect the ductility, yield strength, ultimate tensile strength, or microhardness of metals [41]. These results appear to be applicable to most metals encountered in ECM. In fact, for some metals, e.g. beryllium and tungsten, ECM is claimed to be able to improve these mechanical properties by the removal of surface layers, which have been damaged by conventional machining. (But for these metals, the choice of a suitable ECM electrolyte is another problem, since surface defects produced by ECM may be a source of reduced fatigue strength).

With many metals, mechanical machining raises the fatigue strength by the introduction of compressive stresses to its surface layers. If, after a mechanical operation, a metal undergoes ECM, a reduction in compressive stress should arise through the electrochemical removal of the surface layers. In Figs. 4.18 and 4.19 confirmatory experimental evidence is presented for Nimonic 80A

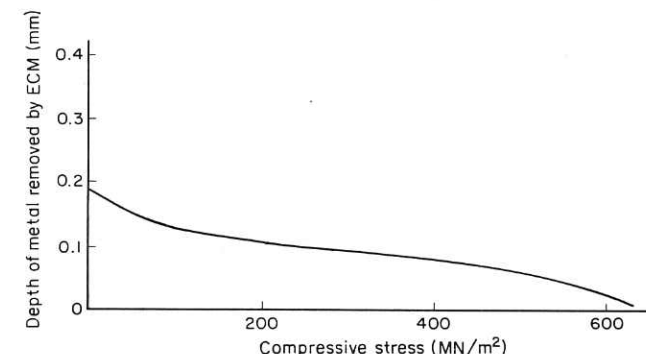


Fig. 4.18 Effect of depth of metal removed upon surface compressive stress (after Evans et al. [42])

machined in NaCl and NaClO₃ solutions [42]. Compressive stresses were found to exist to about 0.2 mm depth (Fig. 4.18). The electrochemical removal of this depth of metal has the effect of reducing the fatigue life to a constant value (Fig. 4.19).

Note that a stress-free surface so produced is one from which the true fatigue strength of the metal can be measured. If, after mechanical machining, the fatigue strength of a metal is reduced by an ECM operation, the required strength can be restored by further mechanical treatment. A sequence of such practices for 403 stainless steel is shown in Table 4.14 [43]. Here, the fatigue strength produced

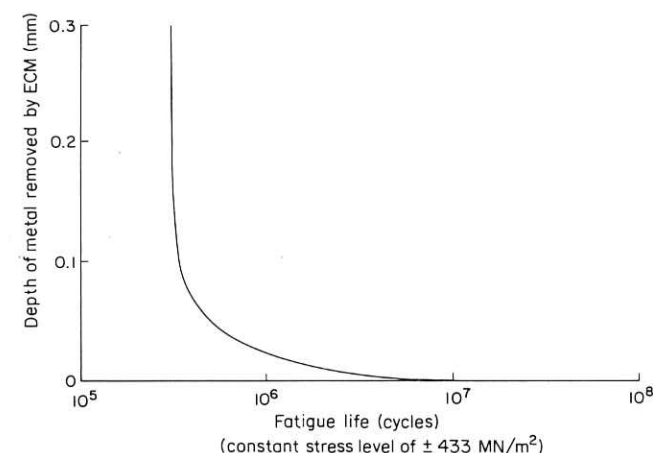


Fig. 4.19 Effect of depth of metal removed upon fatigue life (after Evans et al. [42])

Table 4.14 Effects on various surface finishing operations on fatigue life of 403 stainless steel (after Zimmel [43])

Sequence of surface treatments	Fatigue strength at $3 \cdot 1 \times 10^7$ cycles (MN/m ²)
Mechanical polishing to 0.4 µm surface finish	470
ECM to 0.76-1 µm finish	350
ECM followed by vapour blasting to 0.38-0.51 µm finish	465
ECM followed by glass-bead blast to 0.38-0.51 µm finish	510

by mechanical polishing has been lowered by ECM. After ECM, treatments by vapour blasting and by glass-bead blasting restored the fatigue strength of the metal to its former levels.

The various surface finishes produced by ECM may themselves be sources of reduction in fatigue properties. An examination of effects of this type has been carried out on Nimonic 80A. The surface finishes studied and their conditions of preparation by ECM are summarised in Table 4.15. Micro-examination of brightened

Table 4.15 Fatigue lives produced by different surface finishes at a stress of ± 386 MN/m² (after Evans et al. [42])

Surface finish	Fatigue life (cycles)
Electrochemically polished	4.9×10^5
Etched	4.4×10^5
Intergranular attack	4.25×10^5
Hemispherical pits	3.3×10^5

surfaces and brightened surfaces with grain boundary delineation showed that fatigue cracks usually originate from pits and that, owing to the electrolyte flow, these defects are more severe than those found in electropolishing. Nevertheless, little consequent reduction in fatigue life occurs. Measurements of the depths of intergranular attack showed that these were about 10^{-2} to 10^{-3} mm; again, defects of this type appear to have little effect on metal fatigue.

Related work on the fatigue properties of electrochemically machined titanium alloys has confirmed that pitting and intergranular attack reduces only slightly the fatigue life of these metals [44].

The removal of compressive stress appears to be the main reason for possible reduced fatigue life of metals undergoing ECM. Surface defects caused by the process itself seem to have only effects of secondary importance.

4.10 Effects of ECM on the properties of the electrolyte solution

In this section, we examine the extent to which continual machining affects the bulk properties of the electrolyte solution.

4.10.1 Specific gravity, conductivity, and viscosity

The metallic products of machining are thought to have negligible effect on the bulk specific gravity and conductivity of the solution [2, 45]. Confirmatory evidence is available from tests on a nickel based alloy machined in NaCl electrolyte of bulk specific gravity and specific conductivity 1.17 and $0.16 \text{ ohm}^{-1} \text{ cm}^{-1}$, respectively, at

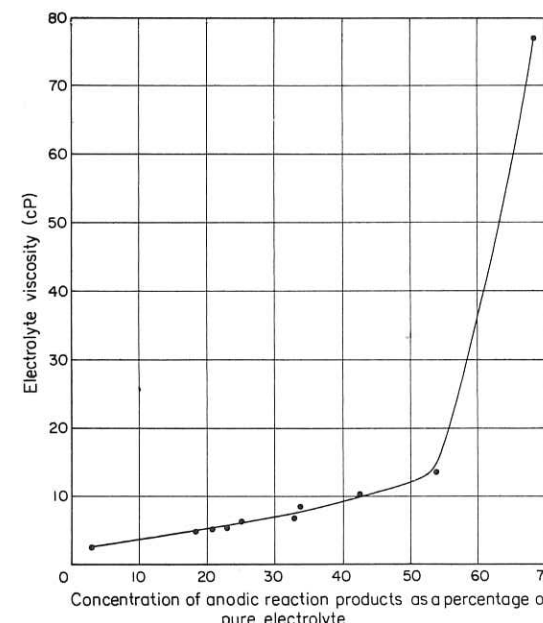


Fig. 4.20 Effect of concentration of anodic metal products on the electrolyte viscosity (after Bayer et al. [45])

24°C; in this work, the anodic debris was present in concentrations ranging from 3 to 70% (v/v) of the electrolyte solution. But the viscosity of the solution does increase with increasing quantities of the anodic products (Fig. 4.20).

4.10.2 pH

That the bulk pH of solutions can change substantially is seen also from Mao's work. For mild steel machined in 2.0M to 4.5M concentrations of NaCl, he reports pH changes from initial values about 6.0 to about 10. These final values indicated the saturation of the solutions with greenish-black coloured Fe(OH)_2 . In NaClO_4 solutions of 2.0M to 4.5M concentrations, the pH changed from about 5.5 to 9. This pH change appeared to be consistent with reaction products of Fe_3O_4 in solution. For 2.0M to 4.5M NaNO_3 solutions, the pH values increased with ECM from about 5.6 to about 11. This substantially higher pH is attributed to the formation of ammonia. This reaction, with the formation of nitrite and hydroxylamine, is preferred to hydrogen gas evolution at the cathode in this electrolyte. For NaClO_3 , the pH values decreased from about 7.8 to about 5.7. This decrease in pH value after ECM could have resulted from a saturated Fe(OH)_3 solution, characterised by its red-brown appearance.

Simple calculations have been carried out which show that, if the effect of a cathode reaction is the release of OH ions into the solution, the pH change may be sufficiently great to cause the precipitation of hydroxides of metals where the pH for precipitation exceeds that of the bulk solution [12]. The authors show that, for typical ECM conditions in which the current is 100 A, the electrolyte velocity is 36 m/s, and the machining region has dimensions $25 \times 25 \times 0.5$ mm³, the pH change decreases with the initial pH; in solutions whose initial pH is about unity, the change in pH is small. But if the initial pH is nearer neutral values, the pH can increase by several units. It is proposed that if a pH of about 8 is required to precipitate nickel hydroxide, a saturated salt solution, with pH 6 to 7, would seem to be unlikely to produce it. But the calculations indicate that the pH will be increased by ECM to cause the precipitation of Ni(OH)_2 .

4.10.3 Ageing

Earlier, the throwing power of NaCl electrolyte solutions was noted to be significantly decreased by the addition of potassium dichromate.

It has been suggested that the presence, in an electrolyte, of increased quantities of chromate ions derived from the chromium present in anode metals can have the effect of reducing the throwing power of electrolyte. This effect could be responsible for the so-called 'ageing' of electrolytes through prolonged use [23].

References

1. Boden, P. J., Brook, P. A. and Evans, J. M., Paper presented at Electrochemical Engineering Symposium, The University, Newcastle upon Tyne, March 1971.
2. McGeough, J. A., Ph.D. Thesis, Glasgow University (1966).
3. Kinoshita, K., Landolt, D., Muller, R. H. and Tobias, C. W., *J. Electrochem. Soc.* (1970) 117, No. 10, 1246.
4. Turner, T. S., Ph.D. Thesis, Nottingham University (1966).
5. Larsson, C. N., Ph.D. Thesis, C.N.A.A. (1968).
6. Cuthbertson, J. W. and Turner, T. S., *The Production Engineer* (1966) May, 270.
7. Mao, K. W., *J. Electrochem. Soc.* (1971) 118, No. 11, 1876.
8. Konig, W. and Degenhardt, H., in *Fundamentals of Electrochemical Machining* (ed. C. L. Faust), Electrochemical Society Softbound Symposium Series, Princeton (1971) p. 63.
9. Bergsma, F., Paper presented at I.S.E.M. Conf., Vienna, October 1970.
10. Mao, K. W., *J. Electrochem. Soc.* (1971) 118, No. 11, 1870.
11. Chikamori, K. and Ito, S., *Denki Kagaku* (1971) 39, 493.
12. Boden, P. J. and Brook, P. A., *The Production Engineer* (1969) Sept., 408.
13. Landolt, D., Muller, R. H. and Tobias, C. W., *J. Electrochem. Soc.* (1969) 116, No. 10, 1384.
14. Hoar, T. P., *Corrosion Sci.* (1967) 1, 341.
15. Reddy, A. K. N., Rao, M. G. B. and Bockris, J. O'M., *J. Phys. Chem.* (1965) 42, 2246.
16. Freer, H. E., Hanley, J. B. and MacLellan, G. D. S., in *Fundamentals of Electrochemical Machining* (see Ref. 8), p. 103.
17. Powers, R. W. and Wilfore, J. F., in *Fundamentals of Electrochemical Machining* (see Ref. 8), p. 135.
18. McGeough, J. A., *Int. J. Prod. Res.* (1971) 9, No. 2, 311.
19. LaBoda, M. A. and McMillan, M. L., *Electrochem. Technol.* (1967) 5, 340, 346.
20. Postlethwaite, J. and Kell, A., *J. Electrochem. Soc.* (1972) 119, No. 10, 1351.
21. Cooper, J., Muller, R. H. and Tobias, C. W., in *Fundamentals of Electrochemical Machining* (see Ref. 8), p. 300.
22. Muller, R. H., Paper presented at First Int. Conf. on ECM, Leicester Univ., March 1973.
23. Brook, P. A. and Iqbal, Q., *J. Electrochem. Soc.* (1969) 116, No. 10, 1458.
24. Chin, D. T. and Wallace, A. J., *J. Electrochem. Soc.* (1971) 118, No. 5, 831.
25. Landolt, D., *J. Electrochem. Soc.* (1972) 119, No. 6, 708.
26. Hoare, J. P., LaBoda, M. A., McMillan, M. L. and Wallace, A. J., *J. Electrochem. Soc.* (1969) 116, No. 2, 199.

27. Hoare, J. P., *Nature* (1968) 219, Sept. 7, 1034.
28. Chin, D. T., in *Fundamentals of Electrochemical Machining* (see Ref. 8), p. 250.
29. Mao, K. W., Hoare, J. P. and Wallace, A. J., *J. Electrochem. Soc.* (1972) 119, No. 4, 419.
30. Chin, D. T., *J. Electrochem. Soc.* (1972) 119, No. 8, 1043.
31. Boden, P. J. and Evans, J. M., *Nature* (1969) 222, 337.
32. Boden, P. J. and Evans, J. M., *Electrochim. Acta* (1971) 16, 1071.
33. LaBoda, M. A., Chartrand, A. J., Hoare, J. P., Wiese, C. R. and Mao, K. W., *J. Electrochem. Soc.* (1973) 120, No. 5, 646.
34. Evans, J. M. and Boden, P. J. in *Fundamentals of Electrochemical Machining* (see Ref. 8), p. 40.
35. Fitz-Gerald, J. M. and McGeough, J. A., Paper presented at I.E.E. Conf. on Electrical Methods of Machining, Forming and Coating, London. Conf. Public. No. 61 (1970) p. 72.
36. Hopenfeld, J. and Cole, R. R., *Trans. A.S.M.E. Series B, J. Eng. Ind.* (1969) Aug., 755.
37. De la Rue, R. E. and Tobias, C. W., *J. Electrochem. Soc.* (1959) Sept., 827.
38. Wagner, C., in *Advances in Electrochemistry and Electro-Chemical Engineering* (ed. P. Delahay and C. W. Tobias), Interscience (1962) 2, 1.
39. Cook, N. H., Loutrel, S. P. and Meslink, M. C., *Increasing ECM Rates*, Mass. Inst. of Tech. Report (1967).
40. Lovering, D. G., Paper presented at 23rd Meeting, I.S.E., Stockholm, Aug.-Sept. 1972.
41. Gurklis, J. A., *Metal Removal by Electrochemical Methods and Its Effect on Mechanical Properties of Metals*, Defence Metals Information Center, Report 213, Battelle Memorial Institute (1965) Jan.
42. Evans, J. M., Boden, P. J. and Baker, A. A., Proc. 12th Int. Mach. Tool Des. Res. Conf., Macmillan (1971) p. 271.
43. Zimmel, L. J., Paper presented at U.S. Nat. Aero- and Space Eng. Meeting, Oct. 1964.
44. Bannard, J., Paper presented at First Int. Conf. on ECM, Leicester Univ., Mar. 1973.
45. Bayer, J., Cummings, M. A. and Jollis, A. U., Gen. Electric Co., Final Report on Electrolytic Machining Development, Rep. No. ML-TDR-64-313 (1964) Sept.

CHAPTER FIVE

Dynamics and Kinematics

Studies of the behaviour of metal-electrolyte combinations for the conditions of ECM must eventually be utilised in applications of the process. In these applications, certain dynamical and kinematic features of the process are invariably exhibited. If one electrode, the cathode, say, is fed towards the other, the width of the gap between the electrodes will eventually become steady.* This equilibrium gap is a consequence of an inherent feature of ECM whereby the rate of forward movement of the cathode becomes matched by the local

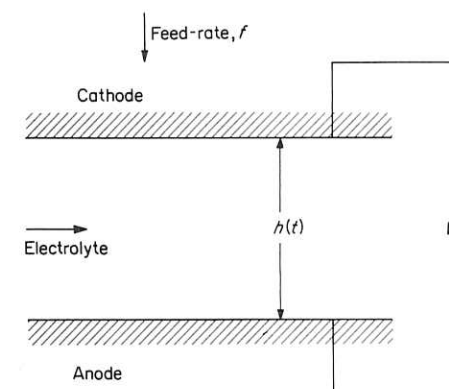


Fig. 5.1 Set of plane parallel electrodes

* The inter-electrode gap referred to here and elsewhere in the text is occasionally referred to as the 'end gap'. Cases in which some other gap is considered should be clear from the discussion at the appropriate part of the text.